

See discussions, stats, and author profiles for this publication at: <https://www.researchgate.net/publication/384277038>

Comprehensive thermal properties, kinetic, and thermodynamic analyses of biomass wastes pyrolysis via TGA and Coats–Redfern methodologies

Article in *Energy Conversion and Management X* · September 2024

DOI: 10.1016/j.ecmx.2024.100723

CITATIONS

7

READS

239

4 authors, including:



Ocident Bongomin

Moi University

47 PUBLICATIONS 706 CITATIONS

[SEE PROFILE](#)



Josphat Igadwa Mwasiagi

Moi University

105 PUBLICATIONS 789 CITATIONS

[SEE PROFILE](#)

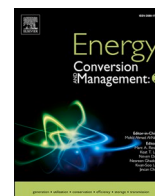


Obadiah Maube

Technical University of Kenya

20 PUBLICATIONS 49 CITATIONS

[SEE PROFILE](#)



Comprehensive thermal properties, kinetic, and thermodynamic analyses of biomass wastes pyrolysis via TGA and Coats-Redfern methodologies

Occident Bongomin^{a,b,c,*}, Charles Nzila^a, Josphat Igadwa Mwasiagi^a, Obadiah Maube^d

^a Department of Manufacturing, Textile and Industrial Engineering, School of Engineering, Moi University, P.O. Box 3900-30100, Eldoret, Kenya

^b Africa Centre of Excellence II in Phytochemical, Textile and Renewable Energy (ACE II-PTRE), Moi University, P.O. Box 3900-30100, Eldoret, Kenya

^c Egypt Solid Waste Management Center of Excellence, Faculty of Engineering, Ain Shams University, Cairo, Egypt

^d School of Mechanical and Manufacturing Engineering, Faculty of Engineering and Built Environment, Technical University of Kenya, P.O. Box 52428-00200, Nairobi, Kenya

ARTICLE INFO

Keywords:

Thermogravimetric analysis (TGA)
Biomass waste
Kinetic modeling
Activation energy
Thermal decomposition
Pyrolysis kinetics
Thermodynamic analysis

ABSTRACT

This study comprehensively analyzes the thermal decomposition characteristics as well as the kinetic and thermodynamic parameters of five biomass wastes, including coffee husk, groundnut shell, macadamia nutshell, rice husk, and tea waste, using Thermogravimetric Analysis (TGA) and the Coats-Redfern method. The TGA experiments were conducted on a PerkinElmer STA 6000 instrument under an inert N₂ atmosphere with a heating rate of 20 °C/min, spanning a temperature range from 25 °C to 950 °C. The results identified three distinct pyrolysis stages: drying, devolatilization, and char formation, with macadamia nutshell demonstrating the highest thermal reactivity and efficient devolatilization characteristics, reflected by its lowest initial devolatilization temperature (175 °C) and highest peak temperature (380 °C). Kinetic analysis revealed that coffee husk had the highest overall activation energy (E_a) of 60.59 kJ/mol, indicating complex thermal degradation behavior. The thermodynamic evaluation showed that coffee husk also exhibited the highest enthalpy change ($\Delta H=55.46$ kJ/mol) but the lowest Gibbs free energy change ($\Delta G=148.34$ kJ/mol), suggesting high energy requirements for decomposition but relatively more spontaneous reactions compared to other biomass types. Macadamia nutshell demonstrated high ΔG (163.24 kJ/mol) and moderate ΔH (32.44 kJ/mol), reflecting greater resistance to spontaneous decomposition. The comprehensive pyrolysis index (CPI) and devolatilization index (D_{dev}) confirmed macadamia nutshell as the most reactive biomass, while rice husk exhibited the lowest reactivity. The findings highlight the importance of multi-step kinetic analysis for accurately understanding pyrolysis processes, providing critical insights for optimizing biomass conversion for energy production. Future research should explore co-pyrolysis with varied biomass mixtures and advanced kinetic modeling to enhance energy yields.

1. Introduction

The ever-increasing global energy demand and the depletion of finite fossil fuel reserves necessitate a shift towards sustainable and environmentally friendly energy sources [1]. Biomass waste, a continuously generated byproduct from agriculture, forestry, and industrial activities, has emerged as a promising renewable energy resource [2,3]. Traditional waste management practices, such as landfilling and incineration, pose significant environmental challenges [4,5]. Landfills occupy valuable land and contribute to soil and water contamination through leachate [6,7]. Incineration reduces waste volume but releases harmful

pollutants, including greenhouse gases, into the atmosphere, adversely impacting air quality and public health [8].

Biomass waste valorization through thermochemical conversion processes like pyrolysis and gasification offers a sustainable solution [9–11]. These processes transform waste into valuable biofuels or chemicals, alleviating the burden on conventional waste disposal methods and promoting a circular bioeconomy [12–14]. Techniques such as Thermogravimetric Analysis (TGA) provide valuable insights into these degradation stages and the kinetics of the process [15,16].

Various kinetic models and reaction mechanisms have been developed to describe the thermal decomposition behavior of biomass including model-free and model-fitting methods [17–19]. The model-

* Corresponding author at: Department of Manufacturing, Textile and Industrial Engineering, School of Engineering, Moi University, P.O. Box 3900-30100, Eldoret, Kenya.

E-mail address: ocident@mu.ac.ke (O. Bongomin).

<https://doi.org/10.1016/j.ecmx.2024.100723>

Received 30 July 2024; Received in revised form 16 September 2024; Accepted 21 September 2024

Available online 23 September 2024

2590-1745/© 2024 The Author(s). Published by Elsevier Ltd. This is an open access article under the CC BY license (<http://creativecommons.org/licenses/by/4.0/>).

Nomenclature*Abbreviation*

<i>CPI</i>	Comprehensive pyrolysis index
<i>FWO</i>	Flynn-Wall-Ozawa
<i>KAS</i>	Kissinger-Akahira-Sunose
<i>TGA</i>	Thermogravimetric Analysis
<i>RM</i>	Total mean reactivity

List of symbols

<i>A</i>	Pre-exponential factor
E_a	Activation energy
T_i	Initial devolatilization temperature
T_p	Peak temperature,

$-R_{p,max}$	Maximum pyrolysis rate
$-R_v$	Average weight loss rate,
D_{dev}	Devolatilization index
R_w	Pyrolysis stability index
ΔH	Changes in enthalpy
ΔG	Changes in Gibbs free energy
ΔS	Changes in entropy
T_f	Final devolatilization temperature
m_∞	Residue weight
R^2	Coefficient of determination
T	Absolute temperature
R	gas constant (8.314 J/mol/K)
$^\circ C$	degree Celsius

free methods include the Flynn-Wall-Ozawa (FWO), Friedman, Starlink and Kissinger-Akahira-Sunose (KAS) methods [20,21]. The model-fitting methods include direct Arrhenius [22], Coats-Redfern [23], Kennedy-Clark [24], Criado master plot [25,26], and Distributed Activation Energy Model (DAEM) methods [27,28]. Model-free methods provide an advantage by not assuming a specific reaction model, allowing for a more flexible analysis across different temperature ranges and heating rates. However, they often require extensive experimental data and can be computationally intensive. The Coats-Redfern method, a model-fitting approach, is widely used due to its simplicity and effectiveness in estimating kinetic parameters such as activation energy and pre-exponential factor [23,29]. This method assumes a first-order reaction model and linearizes the Arrhenius equation, facilitating straightforward calculations from TGA data [22]. By applying the Coats-Redfern method, researchers can obtain reliable kinetic parameters with fewer data points compared to model-free methods, making it an efficient choice for preliminary analysis of biomass pyrolysis [30,31]. The method's ability to provide accurate and consistent results with limited data enhances its applicability in studies aiming to optimize pyrolysis conditions for various biomass materials.

Understanding the kinetic and thermodynamic parameters associated with biomass pyrolysis is crucial for the successful industrialization of this process [32–34]. These parameters provide fundamental insights into the reaction mechanisms, energy requirements, and product distribution, enabling the optimization of reactor design, operating conditions, and product recovery [35,36]. Kinetic parameters, such as activation energy (E_a), pre-exponential factor (A), and reaction order (n), quantify the rate at which biomass undergoes pyrolysis [37–40]. This information is essential for several reasons. Firstly, it aids in reactor design by allowing for the accurate modeling and simulation of pyrolysis reactors, leading to optimized reactor configurations and operating conditions [41–46]. Secondly, understanding the reaction kinetics is vital for process control, enabling precise regulation of process variables like temperature and residence time to achieve desired product yields and qualities [47,48]. Thirdly, accurate kinetic models help predict energy consumption and identify potential energy-saving strategies, enhancing overall energy efficiency [49–52].

Thermodynamic parameters, including enthalpy (ΔH), entropy (ΔS), and Gibbs free energy (ΔG), provide insights into the energy balance and spontaneity of the pyrolysis process [53]. This information is crucial for predicting product yields, as thermodynamic data can estimate the equilibrium yields of different products, aiding in process optimization [26,54]. Additionally, understanding the energy requirements of the pyrolysis process facilitates the integration of heat recovery systems and energy-efficient process design [55]. Thermodynamic analysis also helps assess the feasibility of different biomass feedstocks and identify suitable pyrolysis conditions, ensuring process viability [56,57].

The dynamics between kinetic and thermodynamic parameters is

essential for a comprehensive understanding of the pyrolysis and biomass valorization processes [58,59]. By combining these parameters, researchers and engineers can develop predictive models, optimize reactor performance, and assess the economic feasibility of biomass pyrolysis [60]. This knowledge is critical for the successful commercialization of pyrolysis technologies and the production of high-value products from biomass wastes [61]. Ultimately, the accurate determination of kinetic and thermodynamic parameters contributes to the development of sustainable and efficient biomass conversion processes [62]. This promotes a circular economy and reduces reliance on fossil fuels, paving the way for a more sustainable future [63,64].

Coffee husk, a byproduct of coffee bean processing, represents a significant waste stream globally, with millions of tons produced annually [65]. Its high volatile matter content and comparable heating value to woody biomass make it a potential candidate for biomass conversion [66,67]. Studies have shown that coffee husk degradation begins around 245 °C, with the maximum rate of weight loss observed around 310 °C, indicating the most rapid decomposition of volatile components [66]. Macadamia nutshells, a byproduct of macadamia nut processing, contain cellulose, hemicellulose, lignin, and extractives [68]. These components offer a valuable source of bio-oils, syngas, and biochar depending on the specific pyrolysis conditions. Macadamia nutshells have been found to exhibit high thermal stability, with initial decomposition starting around 220 °C and peak decomposition at 295 °C [69]. The high heating value reinforces its potential as a valuable feedstock for thermochemical conversion processes [70]. Additionally, studies suggest that macadamia nutshells can exhibit synergistic effects when co-pyrolyzed with other waste materials, such as polyethylene terephthalate (PET), leading to increased carbon yield [71].

Rice husk, a byproduct of global rice cultivation, has high cellulose content, making it a valuable feedstock for biofuel production [72,73]. Pre-treatment methods like acid or alkali treatment can improve its conversion efficiency [74]. Studies have shown that rice husk exhibits moderate thermal stability, with decomposition starting around 250 °C and maximum weight loss occurring around 350 °C [72]. Tea waste, rich in various components such as caffeine and polyphenols, offers potential for generating biofuels and valuable biochemicals [75]. Tailoring its pyrolysis behavior through pre-treatment techniques like torrefaction can optimize product yields based on the desired outcome [76]. Groundnut shell, another agricultural residue, has been studied for its pyrolysis kinetics and thermodynamic properties [77]. Research has indicated that groundnut shell exhibits moderate thermal stability, with initial decomposition starting around 230 °C and peak decomposition at 340 °C [16]. Kinetic analysis has shown that groundnut has a relatively low energy barrier for reaction initiation [78,79].

Pyrolysis is a crucial thermal degradation process for converting biomass into valuable products such as biochar, bio-oil, and syngas [80,81]. Despite extensive research, detailed kinetic and

thermodynamic analyses are still needed to optimize these processes. This study aims to address this gap by investigating the pyrolytic behavior of various biomass wastes using TGA and the Coats-Redfern model, providing insights into their potential bioenergy applications.

This study examines the thermal decomposition characteristics and kinetic parameters of five biomass wastes: coffee husk, groundnut shell, macadamia nutshell, rice husk, and tea waste. Using TGA, we aim to understand the thermal behavior and optimize the pyrolysis process for these materials. The primary objectives are to evaluate the initial and peak devolatilization temperatures, maximum pyrolysis rates, and average decomposition rates of the biomass wastes. Additionally, we estimate kinetic parameters including the E_a and A using the Coats-Redfern method. We also assess thermodynamic properties such as ΔH , ΔG , and ΔS . Finally, we compare the thermal stability of the different biomass wastes to identify potential bioenergy applications.

2. Materials and methods

2.1. Materials

The biomass wastes used in this study include coffee husk, groundnut shell, macadamia nutshell, rice husk, and tea waste (Fig. 1). The coffee husk, groundnut shell and macadamia nutshell were obtained from local agricultural processing units, while rice husk and tea waste were collected from rice mills and tea processing facilities, respectively. All biomass samples were selected based on availability, and sourced from sustainable and reliable suppliers to ensure consistency and quality.

2.2. Sample preparation and characterization

The biomass samples were first sun-dried for 2 days, 4 h each day to remove any surface moisture and then ground to a uniform particle size using a laboratory grinder. The ground samples were sieved to obtain particles of size < 1 mm, ensuring homogeneity. The prepared samples were stored in airtight containers to prevent moisture absorption before analysis. The proximate properties of the feedstocks were determined using macro-thermogravimetric analyzer (ELTRA THERMOSTEP Thermogravimetric Analyzer) following ASTM E1131-08 standard [82]. Elemental constituents of feedstocks were determined using CHNS Automatic Analyzer, Elementar-Vaio ELIII, Germany. In addition, Shen et al. [83] model, Parikh model [84], and Genetic Programming (GP)-model [85] were used to determine the elemental composition and compare with the experimental results. The lower heating value (LHV) and higher heating values (HHV) of the biomass were estimated from ultimate properties using the correlation models proposed by Hosokai et al. [86], Channiwalwa & Parikh [87] and Huang & Lo [88]. The proximate and the ultimate/elemental properties of the biomass waste materials are presented in Table 1 and Table 2, respectively.

2.3. Thermogravimetric analysis (TGA)

Following, the wastes were sorted and a study on thermochemical conversion was performed to evaluate the scope of resource recovery. This study discusses the thermal decomposition behaviour of five biomass waste samples through TGA analysis using Perkinmer STA 6000

at a constant heating rate of $20\text{ }^\circ\text{C}/\text{min}$ in an inert N_2 atmosphere with a purge gas flow of $50\text{ mL}/\text{minute}$ from $25\text{ }^\circ\text{C}$ to $950\text{ }^\circ\text{C}$ (Fig. 2). The experiment was conducted with a single heating of $20\text{ }^\circ\text{C}/\text{min}$. The previous study revealed that at this rate, complete degradation of the material can be achieved in lesser time. Moreover, the quality of the data can be higher without much outliers [15]. Approximately $10 \pm 1\text{ mg}$ of each biomass sample was placed in a platinum crucible and heated under the specified conditions. The TGA instrument continuously recorded the weight loss as a function of temperature and time, generating TG and DTG curves for each sample.

2.4. Pyrolysis performance analysis

A variety of characteristic parameters can be used to quantify the performance of any pyrolysis process [89], including the initial devolatilization temperature (T_i), peak temperature (T_p), maximum pyrolysis rate ($-R_p$), average weight loss rate ($-R_v$), comprehensive pyrolysis index (CPI), devolatilization index (D_{dev}) and pyrolysis stability index (R_w). The T_i , which may be estimated using the intersection approach, is the extrapolated onset temperature based on the partial peak caused by the degradation of the hemicellulose. Also, T_i and the final devolatilization temperature (T_f) can be used to compute the average mass loss rate ($-R_v$) [90,91].

2.4.1. Initial devolatilization and peak temperatures

The T_i is the temperature at which the pyrolysis process begins, marking the onset of significant mass loss due to the release of volatile components [79,92]. It is typically estimated using the intersection approach, which involves extrapolating the onset temperature based on the partial peak attributed to the degradation of hemicellulose. This temperature is crucial for understanding the thermal stability of the material and the initiation of pyrolysis reactions. The T_p is the temperature at which the maximum rate of pyrolysis occurs [93]. It indicates the point of the highest thermal decomposition activity and is critical for designing and optimizing pyrolysis processes, as it reflects the most intense phase of biomass breakdown [94].

2.4.2. Maximum decomposition and average weight loss rates

The $-R_p$ is the rate at which decomposition or pyrolysis occurs at its peak, often expressed as a negative value to denote the mass loss rate [95]. This parameter is important for assessing the efficiency and speed of the pyrolysis reaction, providing insights into how quickly the material is being converted into gases, liquids, and char [96]. The $-R_v$ is the parameter that represents the average rate of mass loss over the entire pyrolysis process. It is computed using both the T_i and the T_f , giving an overall measure of the decomposition rate of the material. The average weight loss rate is useful for evaluating the consistency and overall performance of the pyrolysis process [95].

2.4.3. Mean reactivity

The Mean Reactivity (RM) is a crucial parameter for assessing the overall reactivity of a material during the pyrolysis process [97]. The total mean reactivity (RM_{tot}) is the summation of all RM at the different distinct peaks on the DTG curve. This index effectively summarizes how quickly and at what temperature the material undergoes decomposition



Fig. 1. Biomass waste materials: (a) coffee husk, (b) groundnut shell, (c) macadamia nutshell, (d) rice husk, (e) tea waste.

Table 1

Proximate properties of different biomass waste materials.

Feedstock	Moisture (%)	Volatile matter (%)	Fixed carbon (%)	Ash (%)	LHV ^a (MJ/kg)	HHV ^b (MJ/kg)	HHV ^c (MJ/kg)
Coffee husk	8.67	62.90	18.37	10.06	19.85	20.68	19.50
Groundnut shell	6.92	66.24	19.76	7.07	17.32	17.89	17.73
Macadamia nut shell	7.39	68.52	21.06	3.03	20.77	21.46	19.74
Rice Husk	5.90	59.19	15.90	19.01	16.6	16.83	16.42
Tea Waste	5.69	62.95	23.01	8.35	19.41	20.01	18.64

$$LHV^a = 38.2C + 84.9(H - O/8) - 0.62; HHV^b = 0.3491C + 1.1783H + 0.1005S - 0.1034O - 0.0151N - 0.0211Ash.$$

$$HHV^c = 0.3443C + 1.192H - 0.113O - 0.024N + 0.093S.$$

Table 2

Ultimate properties of different biomass waste materials.

Feedstock	Coffee husk (%)	Groundnut shell (%)	Macadamia nutshell (%)	Rice Husk (%)	Tea waste (%)
Parikh model					
Carbon (C)	40.320	42.727	44.389	37.057	43.299
Hydrogen (H)	4.855	5.135	5.343	4.496	5.099
Oxygen (O)	35.523	37.538	39.017	33.006	36.960
Shen model					
Carbon (C)	39.642	42.347	44.602	35.515	42.775
Hydrogen (H)	4.914	5.165	5.336	4.636	5.178
Oxygen (O)	35.513	37.623	39.225	32.727	37.155
GP-model					
Carbon (C)	41.474	43.781	45.787	38.335	45.172
Hydrogen (H)	5.765	5.836	6.005	5.305	5.665
Oxygen (O)	30.871	33.683	35.109	28.707	33.107
Experimental study					
Carbon (C)	50.001	45.680	52.490	40.310	49.980
Hydrogen (H)	6.325	4.910	5.490	4.260	5.003
Oxygen (O)*	32.581	40.763	37.193	34.880	33.956
Nitrogen (N)	0.959	1.523	1.772	1.530	2.679
Sulphur (S)	0.072	0.054	0.025	0.009	0.0350

*Results obtained by difference ($O = 100 - (C + H + N + S + ASH)$).

[97]. A higher RM_{tot} value indicates that the material is highly reactive, decomposing rapidly at relatively lower temperatures [89]. This reactivity is vital for processes aiming to maximize efficiency and throughput, as more reactive materials tend to convert into the desired pyrolysis products more readily. High RM suggests that the pyrolysis process can be conducted at lower temperatures, potentially reducing energy consumption and increasing the overall process efficiency [98]. It was calculated using Eq. (1) [98].

$$RM_{tot} = 100 \sum (R_p / T_p) \quad (1)$$

where R_p represents the maximum pyrolysis rate for each distinct peak, and T_p is the corresponding peak temperature.

2.4.4. Comprehensive pyrolysis index

The CPI is a synthetic parameter designed to encapsulate the overall efficiency and effectiveness of the pyrolysis process [89,99]. This index integrates multiple aspects of the pyrolysis process, including the rate of decomposition and the thermal characteristics of the material [27,100]. A higher CPI value indicates a more efficient pyrolysis process, characterized by high decomposition rates and significant weight loss, while retaining minimal residual mass [91,101]. This comprehensive measure helps in evaluating the overall performance of the pyrolysis process,

guiding optimization for better energy efficiency and product yield. It was defined and calculated using Eq. (2) [98].

$$CPI = \frac{(-R_{p,max})x(-R_v)xM_f}{T_i x T_{p,max} x \Delta T_{1/2}} \quad (2)$$

Where; half-peak width range ($\Delta T_{1/2}$) (when $R/R_p = 1/2$ where R is the decomposition rate), M_f is the weight loss during the entire pyrolysis process ($M_f = m_0 - m_\infty$), $-R_v$ is average decomposition rate, $-R_p$ is the maximum decomposition rate, m_∞ is the residue weight, m_0 is the initial weight in percentage.

2.4.5. Devolatilization index

The Devolatilization Index (D_{dev}) is a measure specifically focused on the rate and extent of volatile component release during pyrolysis [89]. While the exact formula can vary, it typically involves parameters such as the rate of weight loss and the characteristic temperatures associated with devolatilization [92]. This index is crucial for understanding how efficiently the volatile components of the material are being liberated during the pyrolysis process [79]. A higher D_{dev} value signifies a rapid and complete release of volatiles, which is particularly important for processes aimed at maximizing the production of gaseous and liquid products [102]. Efficient devolatilization can enhance the overall yield and quality of these products, making D_{dev} a key parameter for optimizing pyrolysis operations, especially when targeting specific output fractions like bio-oil or syngas. It was estimated using Eq. (3) [98].

$$D_{dev} = \frac{R_{p,max}}{T_i x T_{p,max} x \Delta T_{1/2}} \quad (3)$$

Where; half-peak width range ($\Delta T_{1/2}$) (when $R/R_p = 1/2$ where R is the decomposition rate); $R_{p,max}$ is the maximum decomposition rate, T_i is the initial decomposition temperature, $T_{p,max}$ is the maximum decomposition peak.

2.4.6. Pyrolysis stability index

The Pyrolysis Stability Index (R_w) evaluates the consistency and stability of the pyrolysis process, taking into account the variability in decomposition rates and temperatures [89]. A lower R_w value indicates a more stable pyrolysis process, characterized by consistent decomposition behavior over time and temperature ranges. Stability is a critical factor for industrial applications, as it ensures predictable and reliable production of pyrolysis products [103]. Stable processes are easier to control and optimize, leading to better product quality and process efficiency [27]. By minimizing fluctuations in the pyrolysis process, operators can achieve more uniform and high-quality outputs, which is essential for scaling up pyrolysis technologies for commercial use [104]. Thus, R_w serves as an important index for ensuring process reliability and enhancing the overall robustness of pyrolysis operations. R_w was calculated using Eq. (4). [89].

$$R_w = 8.5875x10^7 x \frac{-R_{p,max}}{T_i x T_{p,max}} \quad (4)$$

where, T_i is the initial decomposition temperature, $T_{p,max}$ is the maximum decomposition peak. $R_{p,max}$ is the maximum decomposition

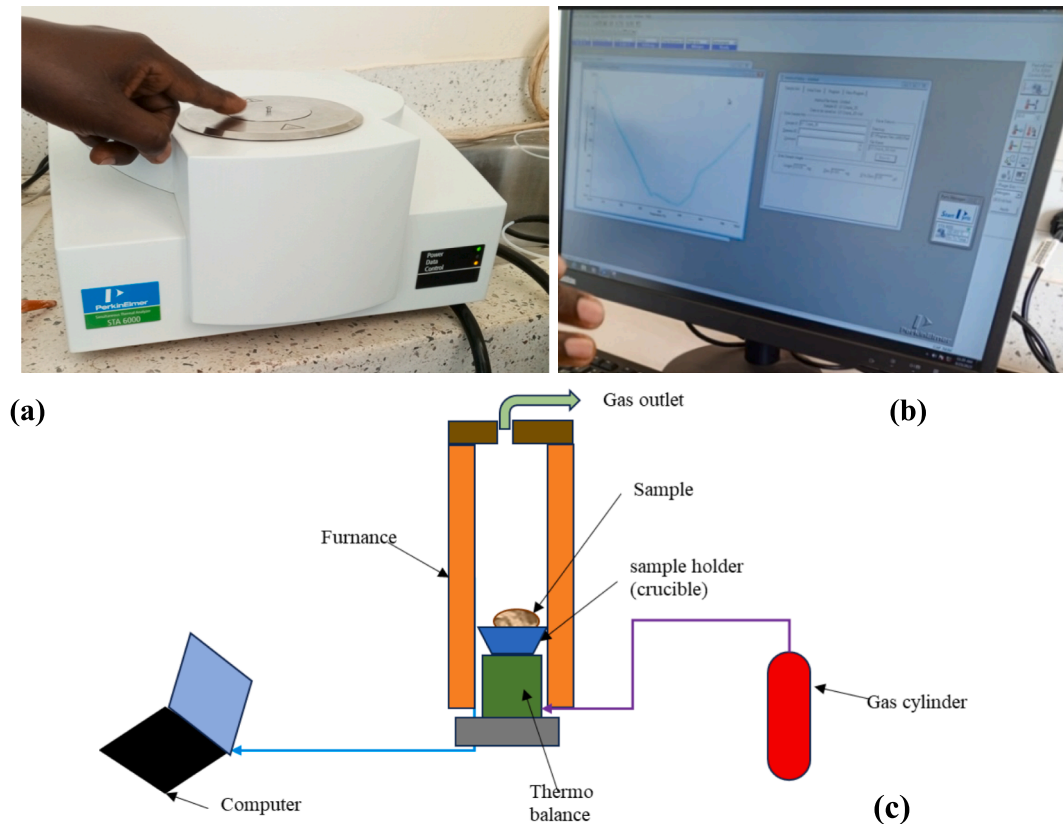


Fig. 2. Experimental setup for thermogravimetric analysis. (a) STA 6000 TGA, (b) computer monitor (c) schematic of TGA.

rate.

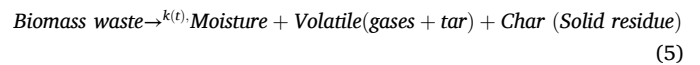
2.5. Coats-Redfern method

The Coats-Redfern method, a widely employed technique for determining kinetic parameters from TGA data, was chosen for this study over advanced isoconversional methods like Flynn-Wall-Ozawa (FWO) and Kissinger-Akahira-Sunose (KAS), which utilize multiple heating rates to offer more detailed insights. This decision was due to the Coats-Redfern method's robustness, simplicity, and effectiveness under non-isothermal conditions typical of biomass pyrolysis [25,31]. By linearizing the Arrhenius equation, the Coats-Redfern method directly estimates the activation energy (E_a , from the slope) and pre-exponential factor (A , from the intercept), providing valuable insights into the thermal decomposition behavior of biomass. This method is particularly suitable for analyzing data from a single heating rate, aligning with the experimental design of our study.

While we acknowledge the concerns raised by Vyazovkin & Muravyev [105] regarding the limitations of single heating rate methods, such as their potential failure to reliably determine kinetic triplets due to the complexities of biomass decomposition, our choice is based on practical considerations. The Coats-Redfern method is ideal for preliminary studies where an approximate understanding of kinetic parameters is needed, allowing for meaningful comparisons across multiple biomass samples under consistent conditions. Moreover, experiments with multiple heating rates require substantial time, resources, and equipment, which may not be feasible. The single heating rate approach also reflects real-world applications where biomass pyrolysis often occurs under constant heating rates, enhancing the relevance of our findings. Despite its limitations, the Coats-Redfern method has demonstrated reliability in numerous studies when used with an awareness of its constraints [106].

2.5.1. Reaction mechanism and kinetic Equations

Biomass waste consists of a complex matrix of biopolymers, with numerous reactions occurring simultaneously during pyrolysis within a given timeframe [107]. This complexity makes predicting the specific reaction mechanisms formed during pyrolysis challenging. To address this, a generalized decomposition reaction is proposed, as shown in Eq. (5).



where k is rate constant, the volatile mean sum of condensable (tar) and non-condensable gasses. The rate constant (k) is dependent on absolute temperature (T), which is expressed by the Arrhenius equation:

The kinetic equation for such heterogeneous system can be written as in Eq. (6).

$$d\alpha/dt = k(t)f(\alpha) \quad (6)$$

where, $d\alpha/dt$ represents rate of degradation. It is a linear function of temperature dependent rate constant, and $f(\alpha)$ is the temperature independent function of conversion, which depends on reaction mechanism.

The normalized conversion (α) is given by Eq. (7).

$$\alpha = \frac{m_0 - m_t}{m_0 - m_\infty} \quad (7)$$

where, m_0 is initial mass of the material, m_t is mass of the material at time t , and m_∞ is the final mass or residue weight of the material after degradation.

Weight loss is given by Eq. (8);

$$\text{Weightloss\%} = \frac{m_0 - m_t}{m_0} \times 100\% \quad (8)$$

The $k(T)$ is rate constant and is expressed by the Arrhenius equation (Eqs. (9) and (10) [108].

$$k(T) = A \exp(-E_a/RT) \quad (9)$$

$$d\alpha/dt = k(T)f(\alpha) \quad (10)$$

The following integral form of Eq. (9) and (10) is given by Eq. (11).

$$g(\alpha) = \int_0^\alpha (d\alpha/f(\alpha)) = A/\beta \int_{T_0}^T \exp(-E_a/RT) dT \quad (11)$$

where, A is pre-exponential factor (min^{-1}), E_a is activation energy (kJ/mol), $k(T)$ is the rate constant, R universal gas constant (0.008314 kJ/mol K), T is the temperature of reaction (K), α is the conversion rate and $f(\alpha)$ is the kinetic model, $g(\alpha)$ is the integral form of the kinetic model.

Coats-Redfern method is employed to find out pre-exponential factor and activation energy by fitting the TGA experimental data (Eq. (12));

$$\ln(g(\alpha)/T^2) = \ln[AR/\beta E_a(1 - 2RT/E_a)] - E_a/RT \quad (12)$$

$$\text{Slope} = -E_a/R \quad (13)$$

$$\text{Intercept} = \ln(AR/\beta E_a) \quad (14)$$

2.5.2. Adoption of multiple reaction mechanism functions

To enhance the accuracy and comprehensiveness of the kinetic analysis, this study employed nine different reaction mechanism functions ($g(\alpha)$) representing various kinetic models, such as order-based chemical reaction, diffusion-controlled, and contracting sphere models, as summarized in Table 3 [109]. Each model captures different aspects of the biomass pyrolysis process, which involves multiple overlapping reactions due to the distinct thermal degradation characteristics of cellulose, hemicellulose, and lignin. Using multiple models allows for a more precise fit to the TGA data, leading to accurate determination of kinetic parameters [39]. This approach provides a comprehensive understanding of the thermal degradation kinetics, enabling the optimization of pyrolysis conditions to maximize energy recovery and improve the efficiency of biomass conversion processes [110].

2.5.3. Significance of activation energy and pre-exponential factor

Activation energy (E_a) is a fundamental kinetic parameter that quantifies the minimum energy required to initiate the decomposition reactions within biomass during thermal degradation [113]. It represents the energy barrier that reactant molecules must overcome for the bonds to break and new products to form. In the context of pyrolysis, activation energy provides insight into the thermal stability of different biomass components. For instance, cellulose, hemicellulose, and lignin each have distinct activation energies, reflecting their varying resistance to thermal decomposition [89,114,115]. The E_a was estimated using slope of the fitted experimental data using Eq. (13). The pre-exponential

factor (A), also known as the frequency factor, is a crucial kinetic parameter in the Arrhenius equation that indicates the frequency of collisions between reactant molecules that lead to a reaction [116]. It provides insight into the number of successful molecular collisions per unit time, which result in the decomposition of biomass [115]. The A value was estimated from intercept of the fitted experimental data using Eq. (14).

2.6. Thermodynamic parameters

These thermodynamic parameters including enthalpy change (ΔH), Gibbs free energy change (ΔG) and entropy change (ΔS) collectively provide a comprehensive understanding of the energy dynamics, spontaneity, and disorder associated with the pyrolysis process. By analyzing these parameters, researchers can optimize the conditions for pyrolysis, improve energy efficiency, and enhance the overall performance and yield of the desired products. The following constants are used in calculation: the Boltzmann constant ($K_B=1.381 \times 10^{-23}$ J/K), Planck's constant ($h = 6.626 \times 10^{-34}$ Js), Gas constant ($R=0.08314$ kJ/mol.K), and the DTG peak temperature (T_p , in Kelvin), respectively [100,117–119]. The ΔH in the context of pyrolysis is a measure of the total energy required to initiate the decomposition process of a material. The ΔH was estimated using Eq. (15).

$$\Delta H = E_a - RT_p \quad (15)$$

Where; R is the universal gas constant, T_p is the peak temperature (in Kelvin), E_a is the minimum energy needed for a chemical reaction to occur.

The Gibbs free energy change (ΔG) is a thermodynamic potential that measures the maximum reversible work obtainable from a thermodynamic system at constant temperature and pressure. ΔG was calculated using Eq. (16).

$$\Delta G = E_a + R.T_p \ln\left(\frac{K_B T_p}{hA}\right) \quad (16)$$

Entropy change (ΔS) is a measure of the disorder or randomness in a system during the pyrolysis process. It was estimated using Eq. (17).

$$\Delta S = \left(\frac{\Delta H - \Delta G}{T_p}\right) \quad (17)$$

2.7. Global single-step and segmented kinetic modeling approaches

This section compares two kinetic modeling approaches used to analyze the pyrolysis process of biomass: the global single-step approach and the multi-step segmented approach. The segmented approach offers a detailed understanding by treating each temperature range as a distinct reaction step with specific kinetic parameters, while the global single-step approach simplifies the entire pyrolysis process as a single reaction with uniform kinetic parameters across the full temperature range [120].

Table 3

The common reaction model for determining the mechanism of biomass degradation [109,109,112].

Reaction model	Reaction mechanism	Code	$f(\alpha)$	$g(\alpha)$
Diffusion	1D diffusion (parabolic rule)	D1	$(2\alpha)^{-1}$	α^2
	2D diffusion (Va lensi equation)	D2	$[-\ln(1-\alpha)]^{-1}$	$(1-\alpha)\ln(1-\alpha) + \alpha$
	3D diffusion (Jander)	D3	$3/2(1-\alpha)^{2/3} [1 - (1-\alpha)^{1/3}]^{-1}$	$[1 - (1-\alpha)^{1/3}]^2$
	3D diffusion (Ginstling-Brounshtein)	D4	$3/2[(1-\alpha)^{-1/3} - 1]^{-1}$	$1 - \frac{2}{3}\alpha - (1-\alpha)^{2/3}$
Geometrical contraction models/ Shape contraction model	Contracting area of sphere	G5	$2(1-\alpha)^{1/2}$	$1 - (1-\alpha)^{1/2}$
	Contracting volume of cylinder	G6	$3(1-\alpha)^{2/3}$	$1 - (1-\alpha)^{1/3}$
Order-based chemical reaction	1st order reaction	R7	$1-\alpha$	$\ln(1-\alpha)$
	2nd order reaction	R8	$(1-\alpha)^2$	$(1-\alpha)^{-1} - 1$
	3rd order reaction	R9	$(1-\alpha)^3$	$1/2[(1-\alpha)^{-2} - 1]$

2.7.1. Multi-step segmented approach

The multi-step segmented approach assumes that each stage of the biomass pyrolysis process, defined by specific temperature ranges or stages, can be treated as a single-step reaction with distinct kinetic parameters [121]. This method accounts for different reaction pathways dominating at various stages of pyrolysis, allowing for a more accurate representation of the decomposition behavior within each stage [107].

To calculate the overall kinetic parameters for the entire temperature range of pyrolysis process, we combined the segmented values using a weighted average approach:

1 Determine the contribution of each Stage

Each stage's fractional weight (w_i) was calculated based on its contribution to total conversion or mass loss using Eq. (18):

$$w_i = \frac{\Delta\alpha_i}{\Delta\alpha_{total}} \quad (18)$$

2 Calculate overall activation energy ($E_{a,overall}$)

The overall activation energy was computed using Eq. (19):

$$E_{a,overall} = \sum_i w_i E_{a,i} \quad (19)$$

Where; $E_{a,i}$ is the activation energy for stage i .

3 Calculate overall Pre-Exponential factor ($A_{overall}$)

The overall pre-exponential factor was determined using a logarithmic average (Eq. (20)).

$$A_{overall} = \exp\left(\sum_i w_i \ln A_i\right) \quad (20)$$

where; A_i is the pre-exponential factor for stage i .

In the multi-step segmented approach, a weighted average is used to combine the activation energies ($E_{a,i}$) from each temperature range, rather than a simple average, to accurately reflect the contribution of each stage to the overall pyrolysis process, ensuring that stages with greater mass loss or conversion have a proportionate impact on the overall kinetic parameters. A simple average would fail to account for these differences, potentially leading to an inaccurate representation of the kinetics [122].

2.7.2. Global single-step approach

The global single-step approach assumes that the entire pyrolysis process can be represented by a single reaction with uniform kinetic parameters across the temperature range. This method simplifies the overall process by considering a single dominant reaction pathway, characterized by a single global activation energy ($E_{a,global}$) and a pre-exponential factor (A_{global}). This approach provides a generalized view of the pyrolysis kinetics, useful for practical applications where a simplified model is sufficient, such as preliminary process design or scaling up [75,94].

3. Results and discussion

3.1. Thermal analysis by TGA and DTG

The thermal degradation behavior of different biomass waste feedstock was investigated using thermogravimetric analysis (TGA) (Fig. 3) and derivative thermogravimetry (DTG) (Fig. 4). The feedstock samples included coffee husk, groundnut shell, macadamia nut shell, rice husk, and tea waste. The results are summarized in Table 4, highlighting the degradation stages, biomass component degradation temperature range, weight loss percentage, peak temperatures (T_p) for each stage, and maximum degradation rate for each stage (DTG_{max} or $R_{p,max}$), initial and

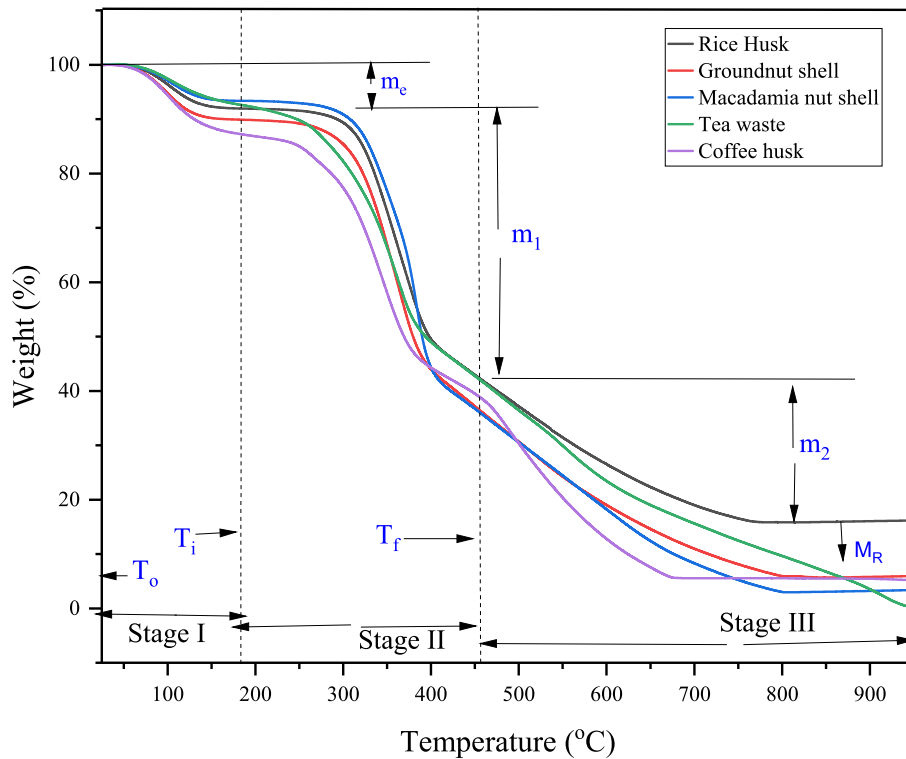


Fig. 3. TGA curves for mass loss during thermal degradation of different biomass waste materials. m_e : mass loss during drying stage, m_1 : mass loss during devolatilization stage, m_2 : mass loss during char formation stage, M_R : residue mass, T_o : starting or ambient temperature, T_i : initial devolatilization process temperature, T_f : final devolatilization process temperature.

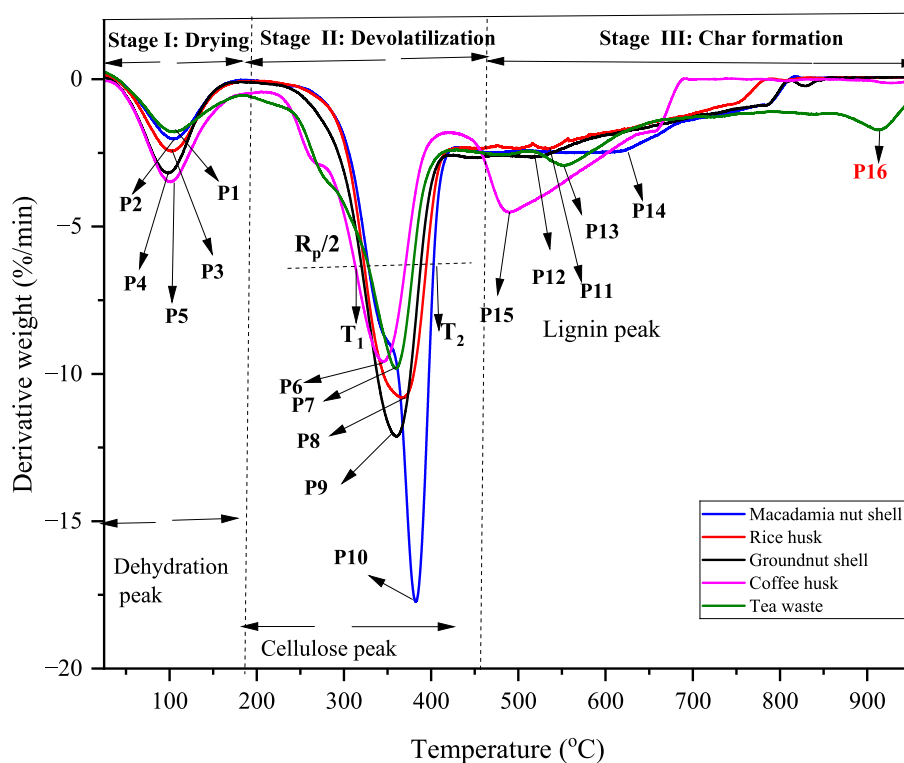


Fig. 4. DTG curves of degradation rate for different biomass materials. (P_1 - P_5): first peak at stage I, (P_6 - P_{10}): second peak (hemicellulose, cellulose peak) at the stage II, (P_{11} - P_{15}): third peak (lignin peak) at stage II. P_{16} : fourth peak (oxidation peak) at the decomposition (stage III). R_p : maximum degradation rate at the main peak, $R_p/2$: half-width peak degradation rate. T_1 : lower end temperature at the intersect of the half-width peak degradation rate, T_2 : upper end temperature at the intersect of the half-width peak degradation rate.

Table 4

Changes in initial and final temperature during the three pyrolysis stages (drying, devolatilization and decomposition) for different biomass waste materials.

Feedstock samples	Degradation Stages	Initial temp. (°C)	Final temp. (°C)	Weight loss (%)	Peak temp. (T_p), °C	DTGmax (%/min) (R_p)	Fractional weight (w)
Coffee husk	Stage 1: Drying	25	215	13.51	100	-3.475	0.142
	Stage 2: Devolatilization	215	425	44.87	345	-9.58	0.473
	Stage 3: Char formation	425	950	36.49	486	-4.483	0.385
Groundnut shell	Stage 1: Drying	25	205	10.22	98	-3.182	0.109
	Stage 2: Devolatilization	205	415	48.79	361	-12.11	0.519
	Stage 3: Char formation	415	950	34.98	516	-2.628	0.372
Macadamia nut shell	Stage 1: Drying	25	175	6.62	103	-2.024	0.069
	Stage 2: Devolatilization	175	440	55.56	382	-17.73	0.575
	Stage 3: Char formation	440	950	34.4	624	-2.404	0.356
Rice husk	Stage 1: Drying	25	180	7.31	101	-2.430	0.087
	Stage 2: Devolatilization	180	435	48.14	369	-10.79	0.575
	Stage 3: Char formation	435	950	28.32	534	-2.360	0.338
Tea waste	Stage 1: Drying	25	185	6.64	109	-1.770	0.067
	Stage 2: Devolatilization	185	430	48.2	358	-9.81	0.484
	Stage 3: Char formation	430	950	44.86	552 and 914	-2.918 and -1.714	0.450

final temperature of each stage.

3.1.1. Drying stage

During the drying or dehydration stage [123], the initial and final temperatures for all biomass materials ranged from 25 °C to approximately 175–215 °C. This stage primarily involves the removal of moisture content, as noted by previous studies [98,124]. Among the materials studied, coffee husk exhibited the highest weight loss at 13.51 %, indicating a higher initial moisture content compared to other materials. Groundnut shell and rice husk followed with weight losses of

10.22 % and 7.31 %, respectively. Macadamia nutshell and tea waste showed the lowest weight losses at 6.62 % and 6.64 %, respectively.

The drying peak temperature (T_p) was relatively low across all materials with minor differences. Macadamia nutshell and tea waste had slightly lower degradation rates (R_p values of -2.024 %/min and -1.770 %/min, respectively), suggesting slower moisture removal compared to coffee husk, which had the highest R_p value of -3.475 %/min.

When comparing these results with previous studies, some interesting observations emerge. For coffee husk, the first peak in the drying

stage (<215 °C) occurred at 100 °C in this study, which is consistent with Nam et al. [66], where the first peak in the dehydration stage (<238 °C) occurred at 110 °C. This similarity is attributed to the evaporation of water in the sample. For macadamia nutshell, Linh et al. [69] reported the drying stage occurring at temperatures below 220 °C, whereas in this study, it occurred at temperatures below 175 °C, indicating a difference in drying temperature ranges.

For groundnut shell, Mishra & Vinu [107] observed the drying stage at temperatures below 150 °C. In contrast, this study found the drying stage occurring at temperatures below 205 °C, suggesting a higher drying temperature range in this analysis. Rice husk, as reported by Kumar et al. [72], had a drying stage at temperatures below 240 °C, whereas this study found it to occur at temperatures below 180 °C, indicating a lower temperature range for moisture removal. Finally, for tea waste, Alashmawy et al. [75] reported the drying temperature at below 196.17 °C, while this study observed drying at temperatures below 185 °C, showing a similar but slightly lower drying temperature range.

3.1.2. Devolatilization stage

The devolatilization stage is characterized by significant thermal degradation and the release of volatiles. In this study, the initial temperatures for this stage ranged from 175 °C to 215 °C, while the final temperatures ranged from 415 °C to 440 °C. Macadamia nutshell exhibited the highest weight loss of 55.56 %, indicating a higher volatile content and greater thermal reactivity. This finding aligns with its proximate analysis. Groundnut shell and tea waste followed closely with weight losses of 48.79 % and 48.2 %, respectively. Coffee husk and rice husk showed slightly lower weight losses of 44.87 % and 48.14 %, respectively. The T_p for devolatilization varied from 345 °C for coffee husk to 382 °C for macadamia nutshell, reflecting different thermal stabilities and decomposition behaviors. Macadamia nutshell also had the highest R_p at -17.73 %/min, indicating rapid decomposition, while coffee husk and tea waste had lower R_p values of -9.58 %/min and -9.81 %/min, respectively.

Comparing these results with previous studies reveals some interesting observations. For coffee husk, the second stage was observed in the temperature range from 215 °C to 425 °C, with a 44.87 % weight loss and a second peak in the DTG curve at 345 °C. This is similar to the findings of Nam et al. [66], who reported the second stage occurring between 238 °C and 400 °C, with a weight loss of 50–60 % and a peak at 310 °C. For groundnut shell, the second stage in this study occurs between 205 °C and 415 °C, whereas Mishra & Vinu [107] reported the second stage spanning 150 °C to 600 °C, involving the decomposition of hemicellulose (200–350 °C) and cellulose (350–600 °C) into lower molecular weight compounds.

For macadamia nutshell, this study found the temperature range for devolatilization to be between 175 °C and 440 °C, with a $T_{p,max}$ at 382 °C. Linh et al. [69] reported a $T_{p,max}$ of 295 °C within a temperature range of 220 °C to 450 °C, indicating a higher maximum peak temperature in the current study. In the case of rice husk, the devolatilization stage in this study occurs between 180 °C and 435 °C, while Kumar et al. [72] reported a range of 240 °C to 500 °C, showing a lower initial temperature for this stage in the present analysis. For tea waste, this study showed an initial temperature (T_i) of 185 °C, a maximum peak temperature ($T_{p,max}$) of 358 °C, and an $R_{p,max}$ of -9.81 %/min. Comparatively, Alashmawy et al. [75] reported T_i , $T_{p,max}$, and $R_{p,max}$ at a heating rate of 20 °C/min as 196.17 °C, 340.47 °C, and -6.97 %/min, respectively, suggesting a slightly lower initial temperature and a higher maximum peak temperature in the current study.

3.1.3. Char formation stage

In the char formation stage, which occurs at higher temperatures ranging from 415 °C to 440 °C initially and up to 950 °C for all materials, the focus is on transforming the remaining solid residue into char. Coffee husk exhibits a significant weight loss of 36.49 % at temperatures above

486 °C. Groundnut shell, macadamia nutshell, and tea waste show weight losses of 34.98 %, 34.4 %, and 44.86 %, respectively. Rice husk has the lowest weight loss at 28.32 %. The peak temperature (T_p) for char formation varies significantly among the materials, with macadamia nutshell showing the highest T_p at 624 °C, indicating higher resistance to thermal degradation. Groundnut shell, rice husk, and tea waste also exhibit high T_p values of 516 °C, 534 °C, and 552 °C, respectively, with tea waste having an additional peak at 914 °C, suggesting complex thermal degradation behavior. The rate of weight loss (R_p) during char formation is generally lower compared to the previous stages, indicating a slower and more gradual char formation process. Groundnut shell and rice husk show the lowest R_p values of -2.628 %/min and -2.360 %/min, respectively. Tea waste, with two R_p values of -2.918 %/min and -1.714 %/min, also indicates a complex and prolonged char formation process.

When comparing these results with previous studies, some interesting observations emerge. For coffee husk, Nam et al. [66] revealed that the third stage of weight loss occurs at higher temperatures above 400 °C, known as the intermediate decomposition along with the thermal degradation of lignin at a lower rate. In this study, it occurs at temperatures above 425 °C, showing a slight shift to higher temperatures. For groundnut shell, Mishra & Vinu [107] reported the third stage occurring at temperatures above 600 °C, whereas in this study, the stage starts at temperatures above 415 °C, indicating a lower temperature range for the char formation stage. For rice husk, Kumar et al. [72] reported the char formation stage occurring at temperatures above 500 °C. In this study, it occurs at temperatures above 435 °C, indicating a lower initial temperature for this stage. Linh et al. [69] reported the char formation stage for macadamia nutshell starting from 450 °C, which is close to the present study's finding of beyond 440 °C. Alashmawy et al. [75] reported the char formation stage for tea waste occurring at temperatures beyond 558.15 °C. In contrast, this study found it occurring at temperatures beyond 430 °C, indicating a lower temperature range for the onset of char formation.

For all pyrolysis stages, the observed similarities, such as the weight loss percentages and the peak temperatures for drying, devolatilization and char formation, indicate consistent thermal behavior across different studies for certain materials. However, discrepancies in the temperature ranges and peak temperatures highlight the variability in biomass characteristics and experimental conditions. These differences could be due to variations in initial moisture content, sample preparation, and heating rates used in different studies.

3.2. Pyrolysis property parameters

Pyrolysis parameters provide critical insights into the thermal degradation behavior of various biomass waste materials [89]. This section discusses key parameters (Table 5), including the mean reactivity (RM), comprehensive pyrolysis index (CPI), devolatilization index (D_{dev}), and pyrolysis stability index (R_w). Understanding these parameters is essential for optimizing pyrolysis processes and improving the efficiency of biomass conversion to bioenergy and biochar.

The RM values for different stages of pyrolysis provide insights into the reactivity of the biomass materials. In stage I, coffee husk has the highest mean reactivity at -3.48 %/min°C, indicating high reactivity at the initial stage of pyrolysis. In contrast, macadamia nutshell shows lower reactivity in stage I at -1.96 %/min°C. In stage II, macadamia nutshell exhibits higher reactivity at -4.64 %/min°C, indicating significant decomposition activity. The total mean reactivity (RM_{tot}) is highest for groundnut shell at -7.11 %/min°C, suggesting it is highly reactive overall, followed by macadamia nutshell at -6.99 %/min°C. The RM_{tot} of groundnut shell is higher than that of other biomasses due to its high volatile matter content, faster decomposition rates, and reactive lignocellulosic structure, which collectively accelerate its thermal degradation during pyrolysis [107]. While tea waste has the lowest RM_{tot} (-4.89 %/min°C) due to its high lignin content, stable char

Table 5
Pyrolysis parameters for different biomass waste materials.

Parameters	Coffee husk	Groundnut shell	Macadamia nutshell	Rice husk	Tea waste
Initial devolatilization temperature (T_i , °C)	215	205	175	180	185
DTG maximum peak temperature ($T_{p,max}$, °C)	345	360	380	368	358
Final devolatilization temperature (T_f , °C)	425	415	440	435	430
Initial devolatilization time (t_i , min)	9.50	9.00	7.50	7.75	8.00
DTG maximum peak time (t_p , min)	16.00	16.75	17.75	17.15	16.65
Final devolatilization time (t_f , min)	20.00	19.50	20.75	20.50	20.25
Residue weight (m_{res} , %)	5.13	6.01	3.42	16.23	0.30
Weight loss for entire pyrolysis (M_f , %)	94.87	93.99	96.58	83.77	99.7
Maximum decomposition rate ($-R_{p,max}$, %/min)	9.56	12.11	17.60	10.80	9.80
Average decomposition rate ($-R_p$, %/min)	4.24	4.57	4.18	3.71	3.87
Half-peak time at the lower intersect of DTG (t_l , min)	13.80	14.65	16.00	14.60	14.25
Half-peak time at the upper intersect of DTG (t_u , min)	17.50	18.15	18.75	18.60	18.00
Half-peak width time range ($\Delta t_{1/2}$, min)	3.70	3.50	2.75	4.00	3.75
Half-peak time at the upper intersect of DTG (T_l , °C)	301	318	345	317	310
Half-peak time at the upper intersect of DTG (T_u , °C)	377	388	400	397	385
Half-peak width temperature range ($\Delta T_{1/2}$, °C)	76	70	55	80	75
Mean reactivity for stage I (RM_1 , %/min°C)	-3.48	-3.25	-1.96	-2.40	-1.62
Mean reactivity for stage II (RM_2 , %/min°C)	-1.00	-3.35	-4.64	-2.92	-2.74
Mean reactivity for stage III (RM_3 , %/min°C)	-0.92	-0.51	-0.38	-0.44	-0.50
Pyrolysis stability index (R_w , 10 ⁹ , %/min°C ²)	1.3	1.8	3.3	1.9	1.6
Devolatilization index (D_{dev} , %/min°C ³)	-1165.9	-1488.6	-2101.9	-1766.4	-1422.3
Total mean reactivity (RMtot, %/min°C)	-5.40	-7.11	-6.99	-5.77	-4.89
Comprehensive pyrolysis index (CPI, 10 ⁻⁵ , % ³ ·°C ⁻³ ·min ⁻²)	68.2	101.0	194.0	63.3	76.1

formation, and lower volatile matter, resulting in a slower overall thermal decomposition rate during pyrolysis.

The *CPI* reflects the overall pyrolysis performance. Macadamia nutshell exhibits the highest *CPI* at $194 \times 10^{-5} \%^3 \cdot ^\circ\text{C}^{-3} \cdot \text{min}^{-2}$, indicating superior overall pyrolysis efficiency and performance. Groundnut shell follows with a *CPI* of $101 \times 10^{-5} \%^3 \cdot ^\circ\text{C}^{-3} \cdot \text{min}^{-2}$, showing good pyrolysis characteristics. Coffee husk, tea waste, and rice husk have lower *CPI* values, indicating moderate to low overall pyrolysis performance. These *CPI* values suggest that macadamia nutshell is the most efficient biomass material for pyrolysis, followed by groundnut shell [89]. The higher *CPI* for macadamia nutshell is due to its higher volatile content, lower ash content, and denser structure, which promote rapid and efficient decomposition during pyrolysis. In contrast, rice husk has a lower *CPI* because of its high silica and ash content, which reduce reactivity and slow down the thermal degradation process.

The D_{dev} indicates the efficiency of devolatilization during pyrolysis. Macadamia nutshell has the most negative D_{dev} value at $-2101.9 \%/\text{min}^\circ\text{C}^3$, indicating highly efficient devolatilization due to its high volatile content and lower ash content, which facilitate rapid thermal decomposition. Additionally, the nutshell's dense structure enables effective heat transfer and rapid release of volatiles, resulting in a more concentrated and efficient devolatilization phase compared to other biomass types. Groundnut shell also shows a high devolatilization efficiency with a D_{dev} value of $-1488.6 \%/\text{min}^\circ\text{C}^3$. Coffee husk and tea waste have moderate D_{dev} values, while rice husk has a relatively lower devolatilization efficiency, indicated by a D_{dev} value of $-1766.4 \%/\text{min}^\circ\text{C}^3$. These differences in D_{dev} values highlight the varying efficiencies of devolatilization for different biomass materials.

The R_w provides insights into the thermal stability of the biomass materials during pyrolysis. Macadamia nutshell has the highest R_w value at $3.3 \%/\text{min}^\circ\text{C}^2$, indicating high thermal stability. Groundnut shell follows with an R_w value of $1.8 \%/\text{min}^\circ\text{C}^2$. Rice husk and coffee husk have similar R_w values around $1.9 \%/\text{min}^\circ\text{C}^2$ and $1.3 \%/\text{min}^\circ\text{C}^2$, respectively. Tea waste has an R_w value of $1.6 \%/\text{min}^\circ\text{C}^2$. These R_w values suggest that macadamia nutshell is the most thermally stable biomass material during pyrolysis, followed by groundnut shell. Macadamia nutshell has the highest R_w due to its complex lignocellulosic structure and lower ash content, allowing it to maintain structural integrity over a broader temperature range. This results in a more gradual decomposition, reflecting greater resistance to thermal degradation [89]. Conversely, coffee husk has the lowest pyrolysis stability index due to its higher hemicellulose content and lower lignin content,

which lead to faster decomposition at lower temperatures, making it less thermally stable during pyrolysis.

In conclusion, the macadamia nutshell exhibits higher *CPI* and R_w compared to other biomass types due to its intense thermal degradation characteristics. It has the highest maximum decomposition rate ($-17.6 \%/\text{min}$) and a narrow half-peak width temperature range (55 °C), indicating a rapid and concentrated pyrolysis reaction. This high reactivity, particularly during the devolatilization stage ($-4.64 \%/\text{min}^\circ\text{C}$), suggests an efficient breakdown of organic matter into volatiles, resulting in a high *CPI* and stability index. Despite its high *CPI* and R_w , the macadamia nutshell has a low residue weight (3.42 %), reflecting a highly efficient conversion process with minimal char remaining [27]. In contrast, tea waste, which has the lowest residue weight (0.3 %), shows lower *CPI* and R_w values due to its slower decomposition rate ($-9.8 \%/\text{min}$) and wider temperature range (75 °C), suggesting a less concentrated and less reactive pyrolysis process. These differences highlight the distinct pyrolysis behaviors of these biomass types, driven by their specific compositions and thermal properties.

3.3. Kinetic analysis

Model fitting is a crucial aspect of analyzing pyrolysis data, as it allows for the quantification and comparison of kinetic parameters across different biomass waste materials including the coffee husk, groundnut shell, macadamia nutshell, rice husk and tea waste. This was done using OriginPro2024b statistical software. By fitting experimental data to various kinetic models, meaningful parameters were extracted which provided insights into the thermal degradation behavior of these biomass materials.

Four different temperature ranges were considered including stage I (drying, 25 °C to T_f), stage II (devolatilization, T_i to T_f), stage III (char formation, T_f to 950 °C), and the full temperature range (25 °C to 950 °C). To estimate the best-fitted reaction model for each stage of biomass pyrolysis and over full range temperature (single-step approach), we applied the Coats-Redfern method and assessed the fit of different reaction models to the TGA data. For each stage of degradation, we calculated the coefficient of determination (R^2) to evaluate the goodness-of-fit of the different reaction mechanism functions and analyzed the residuals to minimize discrepancies between experimental and predicted values. Since biomass pyrolysis is a multi-step process involving overlapping reactions with different thermal stabilities, the best-fitted reaction model varied across different stages as highlighted in

Table 6
Kinetic parameters for different biomass waste materials determine using the Coat-Redfern integral methods.

Reaction Models	Coffee husk			Ground nutshell			Macadamia nutshell			Rice husk			Tea waste		
	A (min ⁻¹)	Ea (kJ/mol)	R ²	A (min ⁻¹)	Ea (kJ/mol)	R ²	A (min ⁻¹)	Ea (kJ/mol)	R ²	A (min ⁻¹)	Ea (kJ/mol)	R ²	A (min ⁻¹)	Ea (kJ/mol)	R ²
Diffusion (Drying stage; Start temperature (25 °C) to Initial devolatilization temperature (Ti))															
D1	6.21E+06	71.3330	0.7898	1.86E+08	82.8000	0.7241	1.83E+10	98.400	0.8201	4.83E+10	99.7102	0.7716	5.29E+08	88.4419	0.7615
D2	3.65E+06	71.7447	0.7920	1.06E+08	83.1371	0.7258	1.00E+10	98.6305	0.8210	2.73E+10	100.0313	0.7841	2.89E+08	88.6680	0.7625
D3	9.54E+05	72.1632	0.7942	2.69E+07	83.4783	0.7275	2.43E+09	98.8625	0.8219	6.88E+09	100.3569	0.7743	6.99E+07	88.8909	0.7637
D4	8.55E+05	71.8841	0.8277	2.46E+07	83.2503	0.7263	2.29E+09	98.7083	0.8213	6.34E+09	100.1468	0.7733	6.56E+07	88.7236	0.7634
Geometrical Contraction (Drying stage; Start temperature (25 °C) to Initial devolatilization temperature (Ti))															
G5	2.55E+02	32.8119	0.7575	2.48E+02	32.8728	0.6979	3.91E+03	41.8753	0.7717	1.53E+03	39.2539	0.7298	2.36E+03	40.9859	0.6263
G6	1.78E+02	32.9163	0.7588	1.72E+02	32.9603	0.6989	2.68E+03	41.9403	0.7724	9.47E+04	39.3460	0.7308	1.61E+03	41.0526	0.6271
Order-based Chemical Reaction (Drying stage; Start temperature (25 °C) to Initial devolatilization temperature (Ti))															
R7	5.80E+02	33.1265	0.7615	5.53E+02	33.1361	0.7013	8.45E+03	42.0708	0.7738	4.94E+03	39.5312	0.7330	5.10E+03	41.1863	0.6290
R8	7.53E+02	33.7675	0.7695	6.87E+02	33.6706	0.7080	9.85E+03	42.4654	0.7779	6.16E+03	40.0930	0.7393	5.96E+03	41.5911	0.6345
R9	9.83E+02	34.4244	0.7774	8.58E+02	34.2157	0.7147	1.15E+04	42.8647	0.7819	7.70E+03	40.6645	0.7458	6.97E+03	42.0008	0.6399
Diffusion (Devolatilization stage; Initial devolatilization temperature (Ti) to Final devolatilization temperature (Tf))															
D1	79.78	39.34	0.9544	222.77	45.833	0.8508	113.49	45.26	0.7663	52.06	40.66	0.7725	113.93	43.26	0.9469
D2	102.92	42.87	0.9534	259.29	49.0480	0.8478	114.81	47.90	0.7631	68.09	43.55	0.7709	112.55	45.76	0.9440
D3	65.45	46.84	0.9517	145.93	52.62	0.8432	55.43	50.82	0.7591	36.14	46.79	0.769	52.23	48.49	0.9406
D4	32.47	44.19	0.9284	78.52	50.23	0.8459	33.03	48.87	0.7617	20.22	44.63	0.7701	31.97	46.67	0.9429
Geometrical Contraction (Devolatilization stage; Initial devolatilization temperature (Ti) to Final devolatilization temperature (Tf))															
G5	0.76	17.59	0.9282	1.31	20.66	0.7893	0.83	20.00	0.6847	0.61	17.89	0.6858	0.78	18.86	0.9182
G6	0.67	18.57	0.9284	1.12	21.55	0.7891	0.68	20.72	0.6850	0.52	18.69	0.6880	0.64	19.53	0.9169
Order-based Chemical Reaction (Devolatilization stage; Initial devolatilization temperature (Ti) to Final devolatilization temperature (Tf))															
R7	3.70	20.62	0.9282	5.69	23.3851	0.7883	3.19	22.23	0.6851	2.56	20.37	0.6915	2.91	20.93	0.9139
R8	25.70	27.49	0.9238	30.74	29.47	0.7828	13.17	27.22	0.6820	12.82	25.95	0.6965	10.03	25.4	0.9033
R9	217.82	35.37	0.9168	196.54	36.39	0.7750	62.82	32.88	0.6758	75.71	32.34	0.6962	45.76	30.56	0.8916
Diffusion (Char formation stage; Final devolatilization temperature (Tf) to 950 °C)															
D1	-4.45E-3	-3.0393	0.1505	-4.10E-3	-2.8207	0.2973	-3.96E-3	-2.6985	0.2529	-5.23E-03	-4.1056	0.4241	6.24E-04	0.3501	0.0145
D2	9.67E-03	3.3209	0.1152	4.16E-02	7.8595	0.9524	6.40E-02	9.6634	0.9868	5.57E-02	8.7365	0.9353	1.81E-02	6.2128	0.8748
D3	2.32E-01	19.1058	0.7127	2.89E-01	20.9901	0.9750	5.08E-01	24.3334	0.9676	5.25E-01	23.7168	0.9647	6.95E-02	16.4177	0.9354
D4	1.20E-02	7.8386	0.3738	1.19E-01	11.8662	0.9922	4.74E-02	14.1466	0.9954	4.37E-02	13.2564	0.9749	1.10E-02	9.3931	0.9457
Geometrical Contraction (Char formation stage; Final devolatilization temperature (Tf) to 950 °C)															
G5	-3.32E-3	-2.2115	0.1241	1.56E-04	0.0785	0.0144	2.96E-03	1.2819	0.9228	2.26E-03	0.9654	0.3702	-2.38E-3	-2.0186	0.6577
G6	3.88E-03	1.8372	0.0723	8.29E-03	3.3593	0.8538	8.33E-03	3.4711	0.8905	1.47E-02	4.7268	0.8404	6.42E-04	0.5128	0.0602
Order-based Chemical Reaction (Char formation stage; Final devolatilization temperature (Tf) to 950 °C)															
R7	7.55E-01	14.0168	0.7277	4.38E-01	12.1854	0.8048	7.18E-01	14.6753	0.8296	8.94E-01	15.2147	0.8114	8.19E-02	6.9604	0.6156
R8	4.36E+05	82.5356	0.8910	4.23E+03	56.6288	0.6574	9.74E+03	62.7875	0.7372	4.39E+04	70.5848	0.6296	7.25E+01	37.2491	0.6176
R9	2.51E+12	171.4493	0.8742	1.84E+12	174.5269	0.7896	8.26E+12	188.104	0.8113	5.36E+12	181.5557	0.8294	7.27E+05	89.1372	0.5831
Diffusion (Full range temperature; Start temperature (25 °C) to 950 °C); Global single step approach															
D1	2.3450	27.0652	0.7184	3.5749	30.0489	0.6968	7.5530	35.3534	0.7896	296.4180	42.6545	0.8349	5.4534	33.6915	0.7717
D2	3.3230	30.1831	0.7795	13.0306	36.5382	0.7644	29.2546	42.1962	0.8404	1138.1110	49.5072	0.8572	6.6336	36.4783	0.8111
D3	4.0529	35.5224	0.8592	9.3430	40.1792	0.8097	19.9607	45.7572	0.8689	787.4701	53.1097	0.8792	4.1821	39.7816	0.8537
D4	1.2510	31.8179	0.8080	4.2270	37.7075	0.7804	9.3430	43.3426	0.8507	364.8730	50.6654	0.8650	2.0625	37.5433	0.8264
Geometrical Contraction (Full range temperature; Start temperature (25 °C) to 950 °C); Global single step approach															
G5	0.1091	11.4478	0.6600	0.1661	12.9718	0.7025	0.2409	15.1402	0.7766	11.9440	23.2346	0.8946	0.0896	11.8556	0.6570
G6	0.1197	12.7906	0.7309	0.1558	13.9059	0.7400	0.2247	16.1159	0.8015	10.9902	24.2234	0.9055	0.0827	12.7696	0.7035
Order-based Reaction (Full range temperature; Start temperature (25 °C) to 950 °C); Global single step approach															
R7	1.2455	16.3180	0.8484	10.2037	161.2618	0.8026	1.4475	18.3888	0.8400	68.4073	26.1059	0.9138	0.5123	14.8741	0.7853
R8	3.04E02	33.4979	0.8306	21.4339	25.2569	0.7991	28.3939	27.7375	0.8209	1.44E03	36.3727	0.8450	7.7957	23.3694	0.8415
R9	2.22E05	55.4796	0.7304	8.62E04	53.6562	0.6578	1.35E05	57.7988	0.6748	1.04E07	68.2814	0.7398	341.4685	36.1779	0.7096
Overall (based on multi-step)	8187.4003	60.5947	–	28.9394	37.3008	–	22.7858	37.8826	–	30.1404	36.5609	–	4.3654	31.1210	–

Table 6. By selecting the model with the highest R^2 value and the smallest residuals for each stage, we ensured that the kinetic parameters accurately reflected the thermal decomposition behavior of the biomass [89]. This approach allowed for a more precise understanding of the kinetics specific to each stage of degradation. The linear fitting curves for different models are observed to have unique patterns for each stage and full temperature range. For instance, Fig. 5 compares the different linear fitting curves for the full temperature range (25 °C to 950 °C) of the different integral models used.

Estimating kinetic parameters across distinct temperature ranges provides a comprehensive understanding of biomass pyrolysis. In the range 25 °C to T_i , parameters reveal the energy required for moisture removal. The range T_i to T_f focuses on the primary decomposition, highlighting volatile release and weight loss, while T_f to 950 °C captures secondary reactions, including char formation from more stable components. Analyzing the full temperature range (25 °C to 950 °C) integrates these stages, offering a complete view of thermal degradation, enabling optimization of conditions for desired yields and product

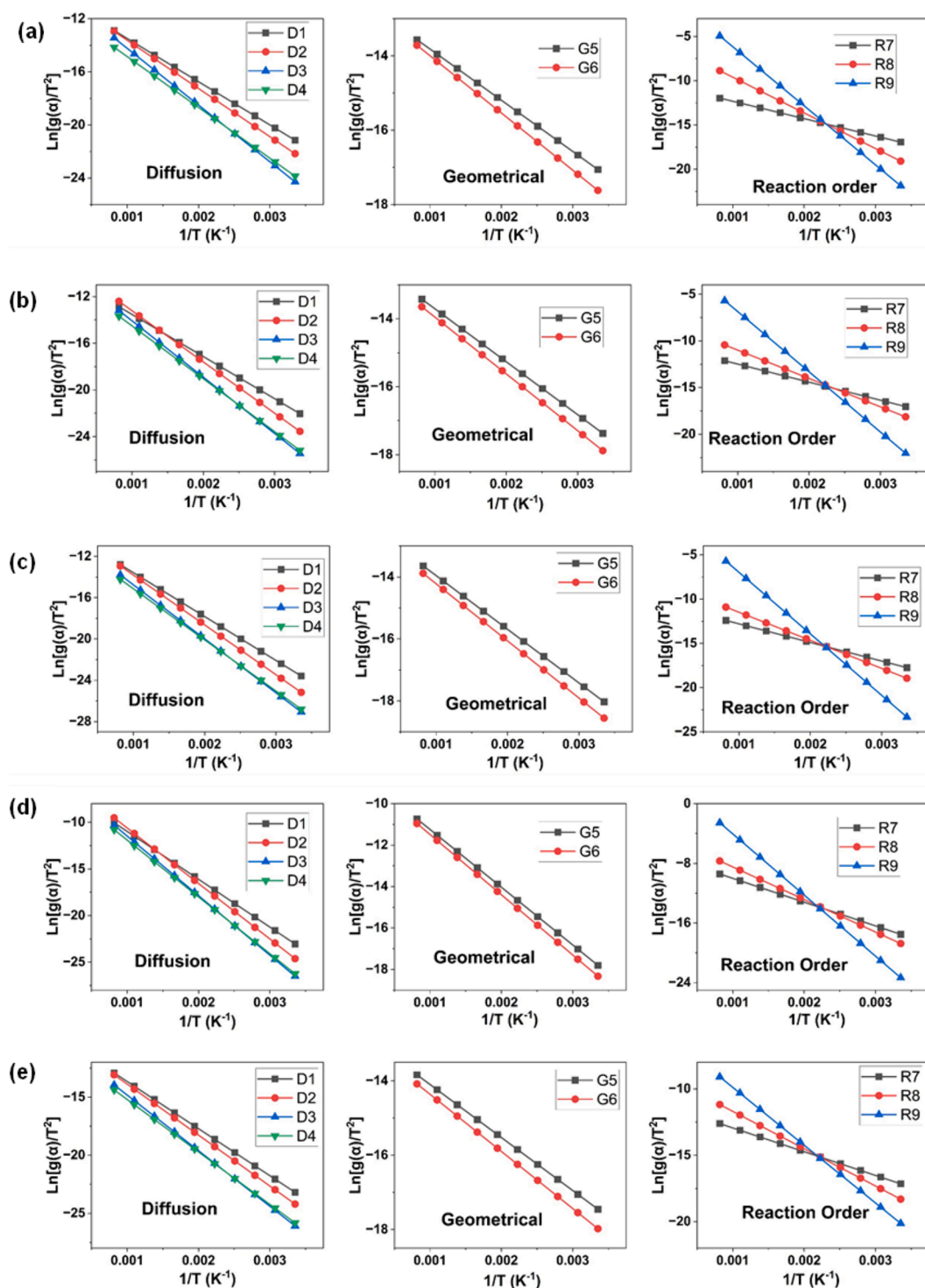


Fig. 5. Fitting curves of the integral method for estimating the kinetic parameters (full temperature range 25 °C to 950 °C) of (a) coffee husk, (b) groundnut shell, (c) macadamia nutshell, (d) rice husk, (e) tea waste.

quality across different biomass types.

3.3.1. Best fit models for coffee husk

For coffee husk, the *D3* diffusion model was the best fit across the full temperature range, with an R^2 value of 0.8592, an E_a of 35.52 kJ/mol, and an A value of 4.05 min^{-1} , indicating that a three-dimensional diffusion mechanism governs the overall pyrolysis process. In drying stage, the *D4* diffusion model was the most suitable, achieving an R^2 of 0.8277, an E_a of 71.88 kJ/mol, and an A of $8.55\text{E}+05 \text{ min}^{-1}$, suggesting a complex diffusion process due to the removal of moisture. During devolatilization stage, the *D1* diffusion model provided the best fit, with an R^2 of 0.9544, an E_a of 39.35 kJ/mol, and an A of 79.78 min^{-1} , reflecting a simpler mechanism as volatiles are released. In char formation stage, the *R8* second-order reaction model was optimal, with an R^2 of 0.8910, an E_a of 82.54 kJ/mol, and an A of $4.36\text{E}+05 \text{ min}^{-1}$, indicating that a reaction-based model better describes the formation of stable char. These results underscore the multi-mechanistic nature of coffee husk pyrolysis.

3.3.2. Best fit models for groundnut shell

For groundnut shell, the *D3* diffusion model provided the best fit over the full temperature range, with an R^2 value of 0.8097, an E_a of 40.18 kJ/mol, and an A of 9.34 min^{-1} , suggesting a three-dimensional diffusion mechanism governs the overall pyrolysis. In drying stage, the *D3* diffusion model also performed best, achieving an R^2 of 0.7275, an E_a of 83.48 kJ/mol, and an A of $2.69\text{E}+07 \text{ min}^{-1}$, indicating it effectively captures the initial moisture removal phase. For devolatilization stage, the *D1* diffusion model was most appropriate, with an R^2 of 0.8508, an E_a of 45.83 kJ/mol, and a high A of 222.77 min^{-1} , suggesting a one-dimensional diffusion mechanism. In char formation stage, the *D4* model again showed the best fit, with an R^2 of 0.9922, an E_a of 11.87 kJ/mol, and an A of 11.9 min^{-1} , reflecting continued diffusion as stable char is formed. This indicates that groundnut shell pyrolysis is characterized by different diffusion mechanisms at various stages, reflecting its complex thermal decomposition.

3.3.3. Best fit models for Macadamia nutshell

For macadamia nutshell, the *D3* diffusion model consistently showed the best fit across all temperature ranges, with an R^2 of 0.8689, an E_a of 45.76 kJ/mol, and an A of 19.96 min^{-1} , indicating a dominant three-dimensional diffusion mechanism. In drying stage, the *D3* diffusion model was also optimal, with an R^2 of 0.8219, an E_a of 98.86 kJ/mol, and an A of $2.43\text{E}+09 \text{ min}^{-1}$, suggesting strong moisture removal characteristics. During devolatilization stage, the *D1* model provided a good fit, with an R^2 of 0.7663, an E_a of 45.26 kJ/mol, and an A of 113.49 min^{-1} , indicating one-dimensional diffusion. In char formation, the *D4* model performed best, with an R^2 of 0.9954, an E_a of 14.15 kJ/mol, and an A of 0.05 min^{-1} , suggesting continued three-dimensional diffusion during char formation. These findings indicate that the pyrolysis of macadamia nutshell is predominantly governed by diffusion processes across all stages.

3.3.4. Best fit models for rice husk

For rice husk, the *R7* first-order reaction model was consistently the best fit across all temperature ranges, achieving an R^2 of 0.9138, an E_a of 26.11 kJ/mol, and an A of 68.41 min^{-1} , pointing to a first-order reaction mechanism throughout the pyrolysis. In drying stage, the *D2* diffusion model showed good performance, with an R^2 of 0.7841, an E_a of 100.03 kJ/mol, and an A of $2.73\text{E}+10 \text{ min}^{-1}$, indicating significant energy requirements for moisture removal. During devolatilization, the *D1* model was suitable, with an R^2 of 0.7725, an E_a of 40.66 kJ/mol, and an A of 52.06 min^{-1} , suggesting one-dimensional diffusion. In char formation, the *D4* model demonstrated the best fit, with an R^2 of 0.9749, an E_a of 13.26 kJ/mol, and an A of 0.04 min^{-1} , indicating continued diffusion as char is formed. These findings highlight the dominant role of diffusion processes in the pyrolysis of rice husk [110].

3.3.5. Best fit models for tea waste

For tea waste, the *D3* diffusion model consistently provided the best fit across all temperature ranges, achieving an R^2 of 0.8537, an E_a of 39.78 kJ/mol, and an A of 4.18 min^{-1} , suggesting that a three-dimensional diffusion mechanism effectively describes its pyrolysis. In drying stage, the *D3* diffusion model was optimal, with an R^2 of 0.7637, an E_a of 88.89 kJ/mol, and an A of $6.99\text{E}+07 \text{ min}^{-1}$, indicating a complex mechanism for moisture removal. During devolatilization stage, the *D1* diffusion model showed a high fit, with an R^2 of 0.9469, an E_a of 43.26 kJ/mol, and an A of 113.93 min^{-1} , pointing to a one-dimensional diffusion mechanism. In char formation, the *D4* model again demonstrated the best performance, with an R^2 of 0.9457, an E_a of 9.39 kJ/mol, and an A of 0.01 min^{-1} , reflecting ongoing diffusion during char formation. Overall, the results suggest that tea waste pyrolysis is predominantly governed by diffusion mechanisms, reflecting its complex thermal decomposition profile [110].

3.4. Kinetic parameters variations across different stages

For drying stage, as shown in Fig. 6a, the E_a and A vary significantly among the biomass types, reflecting their different moisture content and drying characteristics. Rice husk shows the highest E_a (100.03 kJ/mol) and A ($2.73\text{E}+10 \text{ min}^{-1}$), suggesting that it requires more energy to remove moisture due to its dense structure and high silica content, which hinders moisture release. Macadamia nut shell also exhibits high E_a (98.86 kJ/mol) and A ($2.43\text{E}+09 \text{ min}^{-1}$), indicating a substantial energy requirement for drying, likely due to its thicker cell walls and complex structure. In contrast, Coffee husk has the lowest E_a (71.88 kJ/mol) and A ($8.55\text{E}+05 \text{ min}^{-1}$), reflecting easier moisture loss, likely due to its less dense structure. Tea waste and Groundnut shell show moderate E_a and A values, indicating intermediate drying behaviors. These variations highlight the impact of biomass physical properties and structure on their drying kinetics.

During devolatilization, the biomass wastes showed distinct thermal decomposition behaviors. Groundnut shell exhibited the highest E_a (45.83 kJ/mol) and A (222.77 min^{-1}), suggesting a more energy-intensive devolatilization process due to its dense structure (Fig. 6b). Macadamia nutshell had a similar E_a (45.26 kJ/mol) but a lower A value (113.49 min^{-1}), indicating a comparable but slightly less complex decomposition pathway than the groundnut shell. Tea waste displayed a slightly lower E_a (43.26 kJ/mol) but a similar A value (113.93 min^{-1}), suggesting similar reaction kinetics but slightly less energy required for decomposition [98]. In contrast, coffee husk and rice husk had the lowest E_a (39.35 and 40.66 kJ/mol) and A values (79.78 and 62.06 min^{-1}), indicating easier thermal breakdown due to their more accessible structures.

During the char formation stage, coffee husk exhibited the highest E_a (82.54 kJ/mol) and A values ($435,925.57 \text{ min}^{-1}$), suggesting that its thermal degradation is significantly more energy-demanding and kinetically complex (Fig. 6c). This contrasts sharply with the other biomass wastes, which showed much lower E_a and A values, indicating less energy-intensive decomposition [98]. Groundnut shell (11.87 kJ/mol), macadamia nut shell (14.15 kJ/mol), rice husk (13.26 kJ/mol), and tea waste (9.39 kJ/mol) all displayed low activation energies, suggesting easier char formation with less energy required. The very low pre-exponential factors for macadamia nutshell, rice husk, and tea waste also reflect simpler reaction pathways compared to coffee husk.

3.5. Comparison of overall and global kinetic parameters

The kinetic parameters, specifically the E_a and the A , were determined for various biomass feedstocks using two different approaches: the multi-step method (overall kinetic parameters) and the global single-step method (global kinetic parameters) [106,125]. The comparison of these results reveals notable differences in the values obtained, highlighting the distinct decomposition characteristics of each biomass type

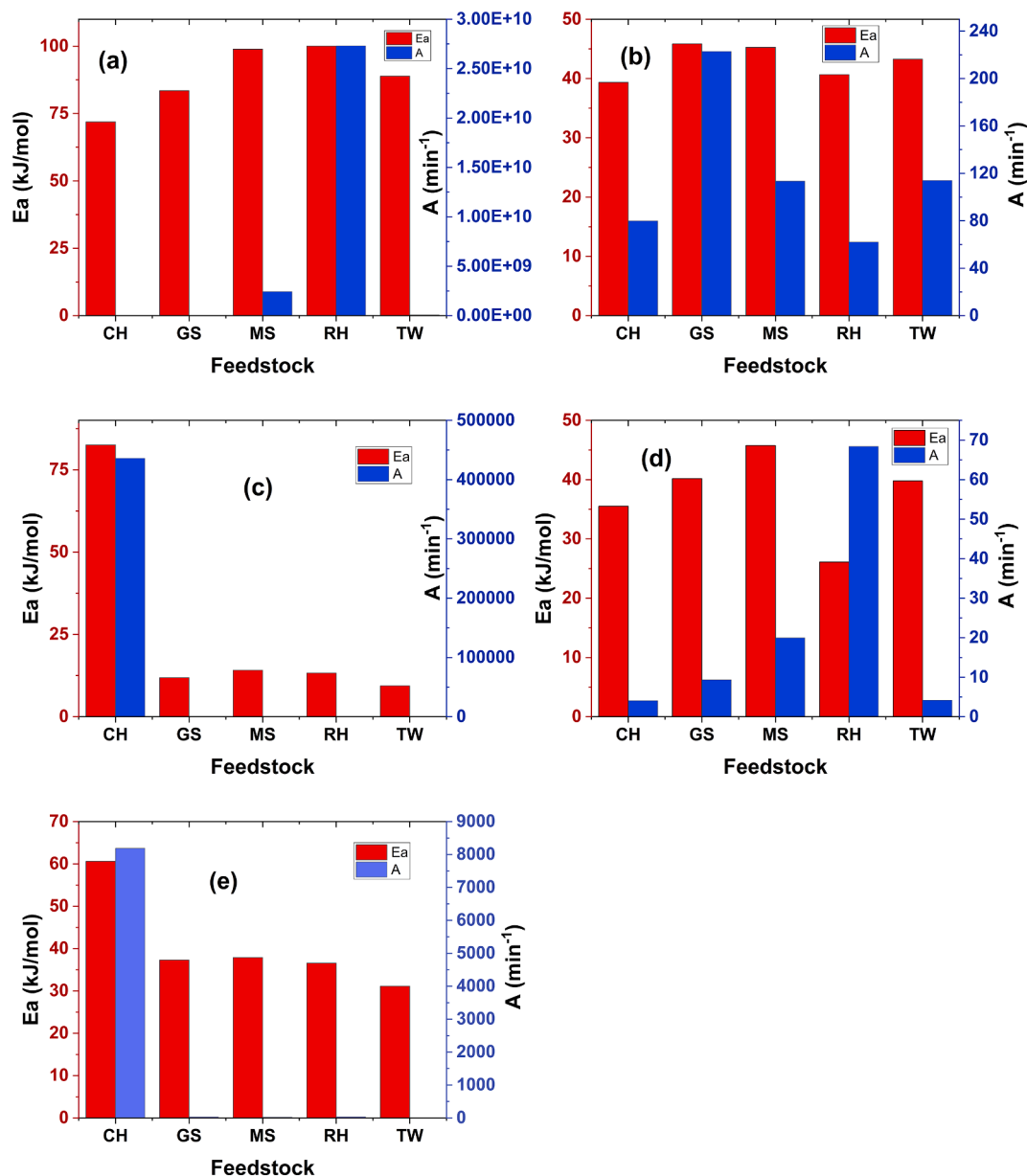


Fig. 6. Comparison of the kinetic parameters of the different biomass waste materials. (a) drying stage, (b) devolatilization stage, (c) char formation stage (d) global single-step approach, (e) overall multi-step approach. CH: coffee husk, GS: groundnut shell, MS: macadamia nutshell, RH: rice husk, TW: tea waste.

and the implications of using different modeling approaches.

3.5.1. Overall and global activation energy

The global single-step approach (Fig. 6d) generally shows lower E_a values for most biomass types compared to the overall multi-step approach (Fig. 6e), highlighting the complexity of the pyrolysis process. For example, coffee husk shows a significantly higher E_a in the multi-step approach (60.59 kJ/mol) than in the single-step (35.52 kJ/mol), indicating multiple reactions with varying energy requirements that are better captured in the multi-step model. This E_a is slightly higher than the 56.60 kJ/mol reported by Alashmawy et al. [75], likely due to differences in experimental conditions and kinetic models.

Groundnut shell and macadamia nutshell show slight differences in E_a between the two approaches, with overall values (37.30 kJ/mol and 37.88 kJ/mol, respectively) being somewhat lower than global values (40.18 kJ/mol and 45.76 kJ/mol). These results align with Collins & Ghodke [126], who reported E_a values of 40.16 kJ/mol and 49.58 kJ/mol, suggesting consistent thermal degradation behavior across studies.

The lower E_a for macadamia nutshell compared to the much higher values for its components reported by Xavier et al. [68] reflects a more integrated, less energy-intensive pyrolysis pathway.

For rice husk, the overall E_a (36.56 kJ/mol) is higher than the global E_a (26.11 kJ/mol), contrasting sharply with the much higher E_a reported by Kumar et al. [72] using different models (219.67–222.19 kJ/mol). This suggests simpler kinetics in the current study. Tea waste shows a lower overall E_a (31.12 kJ/mol) than the global E_a (39.78 kJ/mol), aligning with the findings by Alashmawy et al. [75] that indicated more complex degradation at different heating rates.

The findings indicate that the multi-step approach provides a more detailed understanding of pyrolysis kinetics by capturing varying energy requirements across different stages, while the single-step model offers a simplified, less accurate view of biomass degradation [106].

3.5.2. Overall and global pre-exponential factor

The pre-exponential factor (A) indicates the frequency of molecular collisions leading to decomposition. The multi-step approach often

provides higher overall A values, capturing multiple reaction pathways more effectively than the single-step approach (global A values). For example, coffee husk's overall A value is 8187.40 min^{-1} (Fig. 6e) compared to global A value (4.05 min^{-1} , Fig. 6d). This is lower than the $21,137.18 \text{ min}^{-1}$ reported by Alashmawy et al. [75], suggesting simpler reaction mechanisms under different experimental conditions.

Groundnut shell shows higher overall A value (28.94 min^{-1}) than global A value (9.34 min^{-1}). This contrasts with Collins & Ghodke [126], who reported much higher A values (396.32 min^{-1} and $4.62 \times 10^3 \text{ min}^{-1}$), indicating more complex kinetics under their conditions. Similarly, for macadamia nutshell, the global A value (19.96 min^{-1}) closely matches the overall A value (22.79 min^{-1}), but remains lower than values for specific components reported by Xavier et al. [68].

Rice husk's global A value (68.41 min^{-1}) is higher than overall A value (30.14 min^{-1}), contrasting with much higher values from Kumar et al. [72], suggesting simpler kinetics in this study. For tea waste, both approaches yield similar A values ($\sim 4.3 \text{ min}^{-1}$), but Alashmawy et al. [75] reported much higher values at different heating rates.

These comparisons highlight that the multi-step approach better captures the complex decomposition processes, while the single-step model offers a simplified but less detailed kinetic picture [19,106].

3.6. Thermodynamic analysis

The thermodynamic parameters including enthalpy change (ΔH), Gibbs free energy change (ΔG), and entropy change (ΔS) for various biomass feedstocks were evaluated across different temperature ranges

Table 7
Thermodynamic parameters for different biomass feedstocks.

Biomass waste	T_p , (K)	A (s ⁻¹)	ΔH (kJ/mol)	ΔG (kJ/mol)	ΔS (kJ/mol.K)
Stage I (Drying)					
Coffee husk	373.15	5.13E+07	68.7832	108.8730	-0.1074
Groundnut shell	371.15	1.61E+09	80.3940	109.6151	-0.0787
Macadamia nutshell	376.15	1.46E+11	95.7367	111.3158	-0.0414
Rice husk	374.15	1.64E+12	96.9222	104.8818	-0.0213
Tea waste	382.15	4.19E+09	85.7152	112.8659	-0.0710
Stage II (Devolatilization)					
Coffee husk	618.15	4786.8	34.2032	150.8777	-0.1887
Groundnut shell	634.5	13366.2	40.5573	155.0412	-0.1804
Macadamia nutshell	655.15	6689.4	39.8157	161.9684	-0.1865
Rice husk	642.15	3123.6	35.3237	159.0094	-0.1926
Tea waste	631.15	6835.8	38.0151	155.3838	-0.1860
Stage III (Char formation)					
Coffee husk	759.15	2.62E+07	76.2271	166.5204	-0.1189
Groundnut shell	789.15	712.0	5.3083	168.3569	-0.2066
Macadamia nutshell	897.15	2.84	6.6913	234.1913	-0.2536
Rice husk	807.15	2.62	6.5490	211.0638	-0.2534
Tea waste	825.15	0.661	2.5361	221.2003	-0.2650
Full temperature range (25 to 950 °C)					
Coffee husk	618.15	243.2	30.3856	162.3671	-0.2135
Groundnut shell	634.5	560.6	34.9065	166.1128	-0.2068
Macadamia nutshell	655.15	1197.6	40.3129	171.8308	-0.2007
Rice husk	642.15	4104.4	20.7696	142.9981	-0.1903
Tea waste	631.15	250.9	34.5367	169.2384	-0.2134
Overall (based on multi-steps approach)					
Coffee husk	618.15	491244.0	55.4579	148.3434	-0.1503
Groundnut shell	634.5	1736.4	32.0310	157.2042	-0.1974
Macadamia nutshell	655.15	1367.1	32.4383	163.2355	-0.1996
Rice husk	642.15	1808.4	31.2246	157.8268	-0.1972
Tea waste	631.15	261.9	25.8762	160.3529	-0.2131

using kinetic models (Table 7). These parameters provide insights into the thermal stability and energy requirements of the biomass during pyrolysis [100].

3.6.1. Enthalpy change

Enthalpy change (ΔH) represents the total change in heat content between the reactants and products during the pyrolysis process. This parameter is crucial in determining whether the decomposition process is endothermic or exothermic, as indicated by the sign of ΔH , which can be either positive or negative. Additionally, ΔH is vital for assessing the energy required to convert biomass into bioenergy products, making it an important thermodynamic indicator in bioenergy production [39].

During the drying stage (Fig. 7a), ΔH values reflect the energy required to remove moisture from biomass. Rice husk shows the highest ΔH (96.92 kJ/mol), indicating significant energy demand, likely due to its moisture retention properties [73]. Macadamia nutshell (95.74 kJ/mol) also has a high ΔH , suggesting a dense structure requiring substantial energy for drying. Coffee husk has a lower ΔH (68.78 kJ/mol), indicating less energy is needed for moisture removal, while tea waste (85.72 kJ/mol) and groundnut shell (80.39 kJ/mol) exhibit intermediate values, reflecting moderate energy requirements.

In the devolatilization stage (Fig. 7b), ΔH values decrease, indicating reduced energy requirements as biomass components decompose. Groundnut shell has the highest ΔH (40.56 kJ/mol), suggesting a more energy-intensive devolatilization process. While coffee husk (34.20 kJ/mol) and rice husk (35.32 kJ/mol) have lower values, indicating easier devolatilization. Macadamia nutshell (39.82 kJ/mol) and tea waste (38.02 kJ/mol) show intermediate values, reflecting their more complex decomposition processes.

During the char formation stage (Fig. 7c), ΔH values are minimal, reflecting lower energy requirements as the biomass decomposition nears completion. Coffee husk exhibits a relatively high ΔH (76.23 kJ/mol), suggesting it still requires considerable energy, likely due to stable lignin components. The other biomass types show much lower ΔH values: groundnut shell (5.31 kJ/mol), macadamia nutshell (6.69 kJ/mol), rice husk (6.55 kJ/mol), and tea waste (2.54 kJ/mol), indicating that they require minimal energy for char formation.

When considering the full temperature range (Fig. 7d), ΔH values are lower, representing the average energy requirement across all pyrolysis stages [91]. Macadamia nutshell has the highest ΔH (40.31 kJ/mol), suggesting consistent energy demand throughout the process, while rice husk (20.77 kJ/mol) and coffee husk (30.39 kJ/mol) show lower values, reflecting a more gradual energy requirement [26].

The multi-step approach (Fig. 7e) reveals distinct differences in ΔH values, providing a more detailed understanding of stage-specific energy requirements. Coffee husk shows a higher overall ΔH (55.46 kJ/mol) in the multi-step analysis, indicating that separate stage analysis captures more accurately the energy demand. Similarly, groundnut shell (32.03 kJ/mol), with a ΔH value close to the 29 kJ/mol reported by Xu et al. [127], along with macadamia nutshell (32.44 kJ/mol), rice husk (31.22 kJ/mol), and tea waste (25.88 kJ/mol), show variations in ΔH values. These findings demonstrate that the multi-step approach provides a more detailed understanding of the energy requirements during pyrolysis compared to the single-step method [19].

3.6.2. Gibbs free energy change

Gibbs-Free Energy Change (ΔG) indicates the amount of usable energy available from the feedstock during pyrolysis and is crucial for determining the spontaneity of the decomposition process. A positive ΔG implies that the process is non-spontaneous, requiring external energy input [39]. During the drying stage (Fig. 7a), ΔG values indicate the spontaneity of moisture removal. Tea waste has the highest ΔG (112.87 kJ/mol), suggesting the least spontaneous drying process, possibly due to its structure or moisture content. Macadamia nutshell (111.32 kJ/mol) also shows a high ΔG , reflecting a non-spontaneous drying process likely due to its dense structure. Rice husk, with the lowest ΔG (104.88

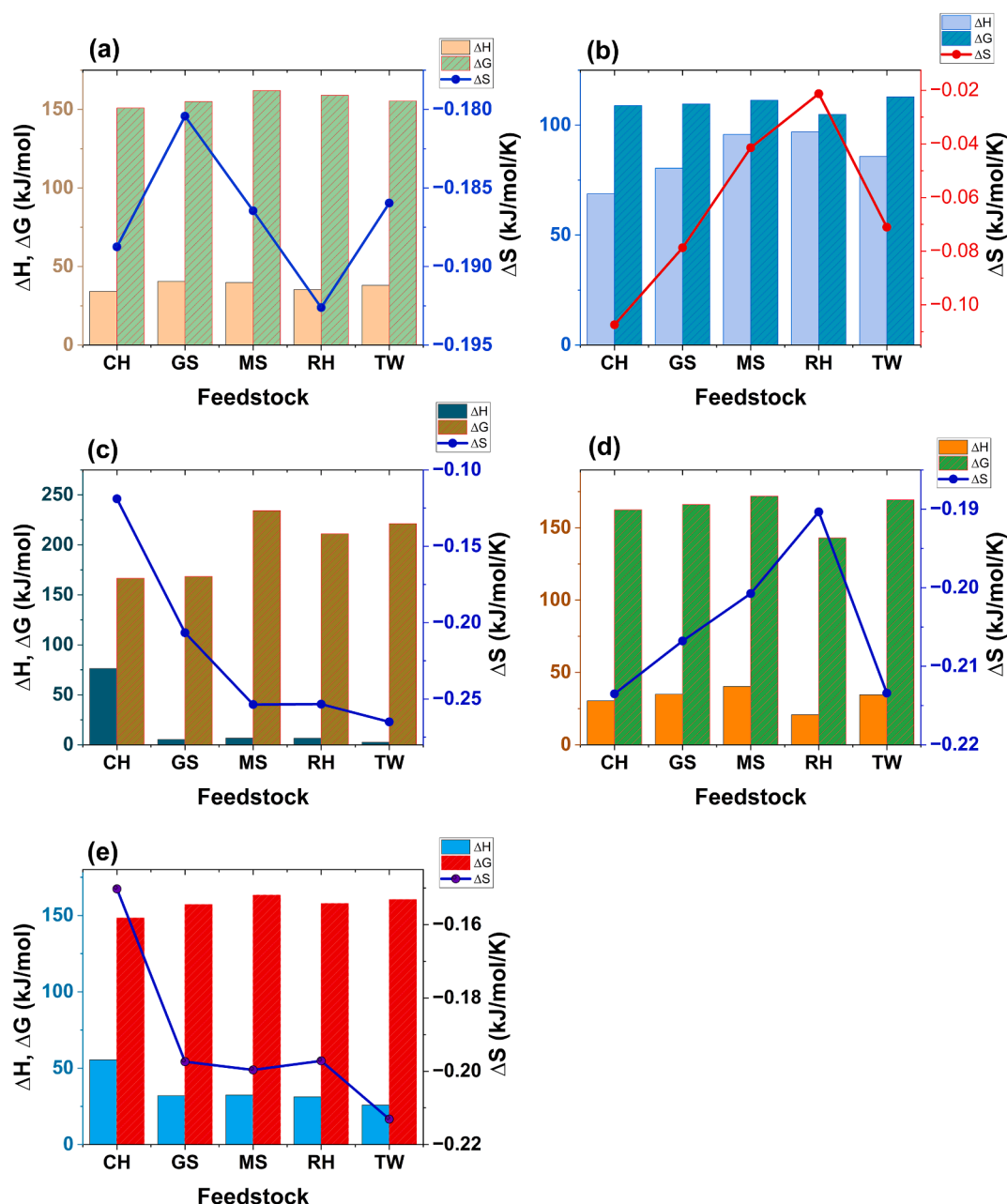


Fig. 7. Comparison of thermodynamic parameters of the different biomass waste materials. (a) drying stage, (b) devolatilization stage, (c) char formation stage, (d) full range temperature (single-step approach), (e) multi-step approach. CH: coffee husk, GS: groundnut shell, MS: macadamia nutshell, RH: rice husk, TW: tea waste.

kJ/mol), indicates a more spontaneous drying, likely due to lower moisture content. Coffee husk (108.87 kJ/mol) and groundnut shell (109.62 kJ/mol) show intermediate spontaneity.

In the devolatilization stage (Fig. 7b), ΔG values increase, reflecting reduced spontaneity as volatiles are released. Macadamia nutshell (161.97 kJ/mol) has the highest ΔG , indicating the least spontaneous devolatilization, likely due to its complex structure. Rice husk (159.01 kJ/mol) and tea waste (155.38 kJ/mol) also exhibit high ΔG , while coffee husk (150.88 kJ/mol) shows the lowest ΔG , suggesting a more spontaneous process.

During the char formation stage (Fig. 7c), ΔG values further rise, indicating non-spontaneity in forming stable char residues. Macadamia nutshell has a very high ΔG (234.19 kJ/mol), suggesting a highly non-spontaneous process due to its dense structure. Tea waste (221.20 kJ/mol) and rice husk (211.06 kJ/mol) also require significant energy, whereas coffee husk (166.52 kJ/mol) and groundnut shell (168.36 kJ/

mol) show relatively lower ΔG values, reflecting more spontaneous char formation.

Across the full temperature range (Fig. 7d), ΔG values provide an overview of pyrolysis spontaneity. Macadamia nutshell (171.83 kJ/mol) and tea waste (169.24 kJ/mol) have the highest ΔG , indicating resistance to thermal degradation, while rice husk (142.99 kJ/mol) has the lowest ΔG , suggesting a more spontaneous decomposition. Coffee husk (162.37 kJ/mol) and groundnut shell (166.11 kJ/mol) show moderate overall spontaneity.

The multi-step approach offers a more detailed perspective on ΔG variations (Fig. 7e), with generally lower values for all types: coffee husk (148.34 kJ/mol), groundnut shell (157.20 kJ/mol), macadamia nutshell (163.24 kJ/mol), rice husk (157.83 kJ/mol), and tea waste (160.35 kJ/mol) than the single-step analysis, indicating increased spontaneity when stage-specific energy requirements are considered. This approach reveals a more accurate depiction of the pyrolysis process, highlighting

the complexities and energy demands of each stage, compared to the simplified single-step analysis [106,125].

3.6.3. Entropy change

Entropy change (ΔS) reflects the degree of disorder or randomness during the pyrolysis process and can be either negative or positive [14]. Negative ΔS values observed across all biomass feedstocks and temperature ranges suggest a decrease in randomness, aligning with the formation of more ordered solid char and gas products from complex biomass structures. During the drying stage (Fig. 7a), all biomass types exhibit negative ΔS values, indicating a decrease in disorder as water is removed [26]. Rice husk shows the least negative ΔS (-0.0213 kJ/mol·K), suggesting minimal reduction in randomness due to its loose structure. Macadamia nutshell (-0.0414 kJ/mol·K) also shows a moderate decrease in entropy, likely due to its dense structure. In contrast, coffee husk (-0.1074 kJ/mol·K), tea waste (-0.0710 kJ/mol·K), and groundnut shell (-0.0787 kJ/mol·K) display more negative ΔS values, reflecting greater entropy reduction due to stabilization of complex structures [106].

In the devolatilization stage (Fig. 7b), ΔS values become more negative, indicating the formation of ordered structures as volatiles are released [91]. Groundnut shell (-0.1804 kJ/mol·K) and tea waste (-0.1860 kJ/mol·K) have less negative value compared to rice husk (-0.1926 kJ/mol·K) and macadamia nutshell (-0.1865 kJ/mol·K), suggesting moderate entropy decreases. Coffee husk shows a slightly more negative ΔS (-0.1887 kJ/mol·K), reflecting significant reorganization.

During char formation (Fig. 7c), ΔS values are highly negative, showing further reduction in disorder as stable char forms. Tea waste (-0.2650 kJ/mol·K) exhibits the most negative ΔS , indicating extensive ordering. Macadamia nutshell (-0.2536 kJ/mol·K) and rice husk (-0.2534 kJ/mol·K) also show significant entropy reductions. Groundnut shell (-0.2066 kJ/mol·K) and coffee husk (-0.1189 kJ/mol·K) have less negative value, suggesting less ordered char formation [128].

For the full temperature range (Fig. 7d), all biomass types maintain negative ΔS values, with tea waste (-0.2134 kJ/mol·K) and coffee husk (-0.2135 kJ/mol·K) showing the greatest overall reduction in randomness. Macadamia nutshell (-0.2007 kJ/mol·K), groundnut shell (-0.2068 kJ/mol·K), and rice husk (-0.1903 kJ/mol·K) indicate varying degrees of entropy reduction.

The multi-step approach (Fig. 7e) offers a detailed view of stage-specific entropy changes. Tea waste shows the most negative overall ΔS (-0.2131 kJ/mol·K), indicating significant entropy reduction. Macadamia nutshell (-0.1996 kJ/mol·K) and rice husk (-0.1972 kJ/mol·K) also exhibit substantial negative changes, while groundnut shell (-0.1974 kJ/mol·K) and coffee husk (-0.1503 kJ/mol·K) show less reduction. These findings underscore the importance of the multi-step approach in capturing detailed entropy changes, reflecting the unique decomposition pathways of each biomass type [125].

3.7. Implications, limitations and future research directions

The findings from this study provide valuable insights into the pyrolysis behavior of various biomass wastes, highlighting the potential for optimizing thermal conversion processes to achieve more efficient energy production and resource recovery. However, certain limitations in the experimental conditions and methodologies suggest areas for improvement. Future research directions are proposed to enhance the applicability and accuracy of these findings, addressing both the methodological limitations and exploring new avenues for biomass utilization.

3.7.1. Implications

Understanding the thermal decomposition characteristics and kinetic parameters of various biomass wastes is crucial for optimizing

pyrolysis processes. By tailoring temperature profiles and heating rates to the specific thermal stability and decomposition rates of different biomass types, more efficient and higher-yielding pyrolysis processes can be developed. The study identifies macadamia nutshells as having the highest thermal stability, indicating their suitability for high-value applications. In contrast, the lower stability of coffee husk and tea waste suggests their potential for faster pyrolysis processes, aiding in the selection of appropriate feedstocks based on desired pyrolysis outcomes.

The calculated *CPI* and D_{dev} values provide a basis for evaluating the efficiency of biomass waste conversion into valuable biofuels and chemicals. For instance, the high *CPI* of macadamia nutshell highlights its potential for efficient resource recovery and waste valorization, contributing to a circular bioeconomy. Optimizing pyrolysis processes based on these findings can lead to more effective biomass waste management, reducing reliance on landfilling and incineration, mitigating environmental pollution, and promoting the generation of renewable energy and bio-based products, aligning with sustainable development goals.

3.7.2. Limitations

The TGA experiments in this study were conducted under controlled laboratory conditions, including a fixed heating rate and an inert atmosphere. However, real-world pyrolysis processes often involve variable conditions, such as fluctuating heating rates, different atmospheric compositions, and the presence of contaminants, which can significantly influence the thermal behavior of biomass wastes. Additionally, this study focused on five specific types of biomass waste, each with unique thermal properties. Although this provides a useful range of insights, the findings may not be entirely generalizable. Further research involving a broader spectrum of biomass types, including less studied or unconventional feedstocks, and larger sample sizes would help enhance the applicability of these results.

Moreover, the Coats-Redfern method employed in this study, while useful for estimating kinetic parameters, assumes a first-order reaction model and linearizes the Arrhenius equation. This simplification may not adequately represent the complex, multi-step kinetics typically observed in biomass pyrolysis, where multiple overlapping reactions and varying activation energies occur. The method's reliance on linearization can also introduce errors, especially in systems with significant deviations from first-order behavior. Therefore, complementary kinetic models or advanced computational techniques may be needed to more accurately capture the intricate decomposition pathways of different biomass materials.

3.7.3. Future research directions

Future research should focus on addressing the limitations identified in this study and further enhancing the understanding of biomass pyrolysis. One key area is the application of advanced kinetic analysis techniques. Utilizing the Criado master plot method can help determine the complex thermochemical reaction mechanisms governing biomass pyrolysis, providing deeper insights into the kinetic behavior of different materials. Additionally, conducting TGA experiments under multiple heating rates and employing advanced isoconversional methods [129], can offer a more accurate determination of kinetic and thermodynamic properties. Comparisons with other model-fitting approaches, like the Distributed Activation Energy Model (DEAM), would also help validate and refine the findings of this study.

Incorporating machine learning approaches, such as Artificial Neural Networks (ANN), represents another promising direction for future research. These models can improve the prediction of kinetic parameters and account for complex, non-linear interactions that traditional models might overlook [26]. By leveraging large datasets and advanced algorithms, machine learning can enhance the understanding of biomass pyrolysis and facilitate the development of more accurate and robust predictive models.

Exploring the thermal decomposition characteristics of biomass

blends is another important area for future research. Investigating combinations of different feedstocks, such as rice husk with macadamia nutshell or coffee husk with groundnut shell, can reveal potential synergistic effects that improve the efficiency and yield of pyrolysis [110,130]. Understanding these interactions can lead to optimized blending strategies, maximizing the advantages of different biomass types and contributing to more sustainable and efficient biomass conversion processes.

Conclusion

This study comprehensively analyzed the pyrolysis behavior of five biomass types including coffee husk, groundnut shell, macadamia nutshell, rice husk, and tea waste through the TGA, kinetic modeling, pyrolysis indices, and thermodynamic assessment across different stages of decomposition. The TGA and DTG analyses indicated that biomass pyrolysis occurs in three stages: drying, devolatilization, and char formation, each with unique weight loss profiles and decomposition rates. These stages highlight the varied thermal stability and reactivity among the biomass types. The *CPI* revealed that macadamia nutshell had the highest overall thermal reactivity ($194 \times 10^{-5} \%^{3.0} \text{C}^{-3} \cdot \text{min}^{-2}$), while rice husk exhibited the lowest ($63.3 \times 10^{-5} \%^{3.0} \text{C}^{-3} \cdot \text{min}^{-2}$), reflecting the energy requirements for decomposition. D_{dev} confirmed the efficiency of macadamia nutshell ($-2101.9 \%/\text{min}^{\circ}\text{C}^3$) in devolatilization, while R_w suggested that macadamia nutshell has the highest stability ($3.3 \%/\text{min}^{\circ}\text{C}^2$) during pyrolysis. Groundnut shell demonstrated the highest total R_m at $-7.11 \%/\text{min}^{\circ}\text{C}$, indicating its rapid thermal decomposition rate compared to other biomass types.

The multi-step kinetic analysis revealed significant variations in the pyrolysis behavior of different biomass types. Coffee husk exhibited the highest E_a (60.59 kJ/mol), indicating a complex and energy-intensive decomposition process, while tea waste showed the lowest E_a (31.12 kJ/mol), reflecting a simpler thermal degradation pathway. The *D3* diffusion model emerged as the best fit for most biomass types, suggesting that three-dimensional diffusion predominantly governs the pyrolysis process, although variations across stages highlight the multi-mechanistic nature of biomass decomposition. Thermodynamic analysis further supported these findings, with coffee husk having the highest ΔH (55.46 kJ/mol) and relatively lower ΔG (148.34 kJ/mol), indicating a high energy demand but moderate spontaneity during pyrolysis. In contrast, macadamia nutshell showed the highest ΔG (163.24 kJ/mol), reflecting less spontaneous decomposition. Tea waste exhibited the most negative ΔS ($-0.2131 \text{ kJ/mol}\cdot\text{K}$), indicating significant structural ordering during pyrolysis, while coffee husk had the least negative ΔS , suggesting minimal reorganization.

CRedit authorship contribution statement

Ocident Bongomin: Writing – review & editing, Writing – original draft, Visualization, Validation, Project administration, Methodology, Investigation, Formal analysis, Data curation, Conceptualization. **Charles Nzila:** Writing – review & editing, Validation, Supervision, Resources, Funding acquisition, Conceptualization. **Josphat Igadwa Mwasiagi:** Writing – review & editing, Validation, Supervision, Resources, Funding acquisition, Data curation, Conceptualization. **Obadiah Maube:** Writing – review & editing, Validation, Supervision, Resources, Investigation.

Declaration of competing interest

The authors declare that they have no known competing financial interests or personal relationships that could have appeared to influence the work reported in this paper.

Data availability

Data will be made available on request.

Acknowledgements

The authors gratefully acknowledge Africa Centre of Excellence II in Phytochemical, Textiles and Renewable Energy (ACE II-PTRE) at Moi University, for providing financial and technical support for this research. The authors also acknowledge the financial support from Strengthening Mobility and Promoting Regional Integration of Engineering Education in Africa (SPREE) program through PHD credit-seeking scholarship awarded to Mr. Ocident Bongomin at Ain Shams University.

References

- [1] Bongomin O, Nziu P. A critical review on the development and utilization of energy systems in Uganda. *Scient World J* 2022;2022:1–25. <https://doi.org/10.1155/2022/2599467>.
- [2] Reddy KV, Satya Sree NR, Ranjit P, Maddela NR. Chapter 23 - Biomass waste and feedstock as a source of renewable energy. In: Shah MPBT-GA to AF for a SF, editor., Elsevier; 2023, p. 325–34. Doi: 10.1016/B978-0-12-824318-3.00033-3.
- [3] Alper K, Tekin K, Karagöz S, Ragauskas AJ. Sustainable energy and fuels from biomass: a review focusing on hydrothermal biomass processing. *Sustain Energy Fuels* 2020;4:4390–414. <https://doi.org/10.1039/d0se00784f>.
- [4] Mpungu IL, Maube O, Nziu P, Mwasiagi JI, Dullo B, Bongomin O. Optimizing Waste for Energy: Exploring Municipal Solid Waste Variations on Torrefaction and Biochar Production. *Int J Energy Res* 2024;2024:36. <https://doi.org/10.1155/2024/4311062>.
- [5] Owino CA, Lubwama M, Yiga VA, Were F, Bongomin O, Serugunda J. Mechanical and thermal properties of composite carbonized briquettes developed from cassava (*Manihot esculenta*) rhizomes and groundnut (*Arachis hypogaea*. L.) stalks with jackfruit (*Artocarpus heterophyllus*) waste as binder. *Discover Applied Sciences* 2024;6. <https://doi.org/10.1007/s42452-024-06123-6>.
- [6] Abdel-Shafy HI, Mansour MSM. Solid waste issue: sources, composition, disposal, recycling, and valorization. *Egypt J Pet* 2018;27:1275–90. <https://doi.org/10.1016/j.ejpe.2018.07.003>.
- [7] Abubakar IR, Maniruzzaman KM, Dano UL, AlShihri FS, AlShammari MS, Ahmed SMS, et al. Environmental sustainability impacts of solid waste management practices in the global south. *Int J Environ Res Public Health* 2022; 19. <https://doi.org/10.3390/ijerph191912717>.
- [8] Ferronato N, Torretta V. Waste mismanagement in developing countries: a review of global issues. *Int J Environ Res Public Health* 2019;16. <https://doi.org/10.3390/ijerph16061060>.
- [9] Okot DK, Bilsborrow PE, Phan AN. Thermo-chemical behaviour of maize cob and bean straw briquettes. *Energy Convers Manage*: X 2022;16:100313. <https://doi.org/10.1016/j.ecmx.2022.100313>.
- [10] Bongomin O, Nzila C, Mwasiagi JI, Maube O. Exploring insights in biomass and waste gasification via ensemble machine learning models and interpretability techniques. *Int J Energy Res* 2024;2024. <https://doi.org/10.1155/2024/6087208>.
- [11] Elhenawy Y, Fouad K, Bassyouni M, Al-Qabandi OA, Majozi T. Yield and energy outputs analysis of sawdust biomass pyrolysis. *Energy Convers Manage*: X 2024; 22:100583. <https://doi.org/10.1016/j.ecmx.2024.100583>.
- [12] Omol DK, Acaye O, Okot DF, Bongomin O. Production of fuel oil from municipal plastic wastes using thermal and catalytic pyrolysis. *J Energy Res Rev* 2020;4: 1–8. <https://doi.org/10.9734/jenrr/2020/v4i230120>.
- [13] Kalak T. Potential use of industrial biomass waste as a sustainable energy source in the future. *Energies* 2023;16:1783. <https://doi.org/10.3390/en16041783>.
- [14] Mariyam S, Parthasarathy P, Pradhan S, Al-Ansari T, McKay G. Co-pyrolysis of biomass and binary single-use plastics: synergy, kinetics, and thermodynamics. *Int J Sustain Energy* 2024;43. <https://doi.org/10.1080/14786451.2023.2168003>.
- [15] Vyas R, Swaminathan P, Chakraborty S, Kiran B. Study on enhancing waste PVC management through predictive Machine Learning analysis of TGA and its economic benefits. *Energy Convers Manage*: X 2024;22:100556. <https://doi.org/10.1016/j.ecmx.2024.100556>.
- [16] Balsora HK, Kartik S, Rainey TJ, Abbas A, Joshi JB, Sharma A, et al. Kinetic modelling for thermal decomposition of agricultural residues at different heating rates. *Biomass Convers Biorefin* 2023;13:3281–95. <https://doi.org/10.1007/s13399-021-01382-4>.
- [17] Najafi H, Rezaei Laye Z, Sobati MA. Thermal conversion potential of tea stems: experimental investigation, reaction mechanism, and kinetic modeling. *Ind Crop Prod* 2024;207:117753. <https://doi.org/10.1016/j.indcrop.2023.117753>.
- [18] Steven S, Hernowo P, Nadirah N, Febjanto I, Herdioso R, Dharmawan D, et al. Transformation method in determining kinetic parameters of biomass thermal decomposition from solid-state approach to volatile state approach. *Biomass Bioenergy* 2024;183:107171. <https://doi.org/10.1016/j.biombioe.2024.107171>.
- [19] Fischer O, Lemaire R, Bensakhria A. Thermogravimetric analysis and kinetic modeling of the pyrolysis of different biomass types by means of model - fitting,

- model - free and network modeling approaches. *J Therm Anal Calorim* 2024. <https://doi.org/10.1007/s10973-023-12868-w>.
- [20] Arumugam DB, Ganesan MC. Catalytic co-pyrolysis of bauhinia purpurea seed and waste medical plastics for sustainable biofuel production: Kinetic analysis and prediction modeling. *Process Saf Environ Prot* 2024;189:374–86. <https://doi.org/10.1016/j.psep.2024.06.040>.
- [21] Wang Y, Yang S, Bao G, Wang H. Investigation on prospective bioenergy from pyrolysis of macadamia nut shell waste using multicomponent Fraser-Suzuki kinetic model, kinetic triplet and thermodynamic parameters. *J Energy Inst* 2024;114:101611. <https://doi.org/10.1016/j.joei.2024.101611>.
- [22] Kumar Shrivastava D, Prasad CJ. Estimation of kinetic and thermodynamic parameters during thermal decomposition of raw, boiled, and torrefied banana peel through arrhenius and CR methods. *Therm Sci Eng Progr* 2024;53:102696. <https://doi.org/10.1016/j.tsep.2024.102696>.
- [23] Ferfari O, Belaadi A, Bourchak M, Gheraout D, Ajaj RM, Chai BX. Thermal decomposition of Syagrus romanzoffiana palm fibers: Thermodynamic and kinetic studies using the coats-redfern method. *Renew Energy* 2024;231:120928. <https://doi.org/10.1016/j.renene.2024.120928>.
- [24] Li B, Ng J-H, Woon KS, Chong WWF, Ng KLA, Lee CT, et al. Comparative analysis of kinetic model-fitting methods and selection priority for horse manure pyrolysis. *Sustain Chem Pharm* 2024;39:101590. <https://doi.org/10.1016/j.scp.2024.101590>.
- [25] Li BY, Tee MY, Nge KS, Ng AKL, Chong WWF, Ng JH, et al. Comparison kinetic analysis between coats-redfern and criado's master plot on pyrolysis of horse manure. *Chem Eng Trans* 2023;106:1273–8. <https://doi.org/10.3303/CET23106213>.
- [26] Choudhary J, Kumar A, Alawa B, Chakma S. Optimization and prediction of thermodynamic parameters in co-pyrolysis of banana peel and waste plastics using AIC model and ANN modeling. *Energy Nexus* 2024;14:100302. <https://doi.org/10.1016/j.nexus.2024.100302>.
- [27] Escalante J, Chen WH, Tabatabaei M, Hoang AT, Kwon EE, Andrew Lin KY, et al. Pyrolysis of lignocellulosic, algal, plastic, and other biomass wastes for biofuel production and circular bioeconomy: a review of thermogravimetric analysis (TGA) approach. *Renew Sustain Energy Rev* 2022;169:112914. <https://doi.org/10.1016/j.rser.2022.112914>.
- [28] Fatmawati A, Nurtono T, Widjaja A. Thermogravimetric kinetic-based computation of raw and pretreated coconut husk powder lignocellulosic composition. *Bioresour Technol Rep* 2023;22:101500. <https://doi.org/10.1016/j.biteb.2023.101500>.
- [29] Tariq R, Saeed S, Riaz M, Saeed S. Kinetic and thermodynamic evaluation of almond shells pyrolytic behavior using Coats-Redfern and pyrolysis product distribution model. *Energy Sour Part A* 2023;45:4446–62. <https://doi.org/10.1080/15567036.2023.2202639>.
- [30] Coats and Redfern. Kinetic parameter Coats and Redfern. *Nature* 1964;201:68–9.
- [31] Ebrahimi-Kahrizangi R, Abbasi MH. Evaluation of reliability of Coats-Redfern method for kinetic analysis of non-isothermal TGA. *Trans Nonferrous Metals Soc China (eng Ed)* 2008;18:217–21. [https://doi.org/10.1016/S1003-6326\(08\)60039-4](https://doi.org/10.1016/S1003-6326(08)60039-4).
- [32] Guo X, Xu Z, Zheng X, Jin X, Cai J. Understanding pyrolysis mechanisms of corn and cotton stalks via kinetics and thermodynamics. *J Anal Appl Pyrol* 2022;164:105521. <https://doi.org/10.1016/j.jaap.2022.105521>.
- [33] Sivaraman S, Shanmugam SR, Veerapandian B, Venkatachalam P. Understanding the pyrolysis kinetics, thermodynamic, and environmental sustainability parameters of Sesamum indicum crop residue. *Environ Res Commun* 2023;5. <https://doi.org/10.1088/2515-7620/ad16f2>.
- [34] Wang S, Wu K, Yu J, Luo B, Chu C, Zhang H. Kinetic and thermodynamic analysis of biomass catalytic pyrolysis with nascent biochar in a two-stage reactor. *Combust Flame* 2023;251:112671. <https://doi.org/10.1016/j.combustflame.2023.112671>.
- [35] Quintero-Naucil M, Salcedo-Mendoza J, Solarte-Toro JC, Aristizábal-Marulanda V. Assessment and comparison of thermochemical pathways for the rice residues valorization: pyrolysis and gasification. *Environ Sci Pollut Res* 2024. <https://doi.org/10.1007/s11356-024-32241-0>.
- [36] Wang K, Shan T, Li B, Zheng Y, Xu H, Wang C, et al. Study on pyrolysis characteristics, kinetics and thermodynamics of waste tires catalytic pyrolysis with low-cost catalysts. *Fuel* 2024;356:129644. <https://doi.org/10.1016/j.fuel.2023.129644>.
- [37] Okot DK, Bilsborrow PE, Phan AN, Manning DAC. Kinetics of maize cob and bean straw pyrolysis and combustion. *Heliyon* 2023;9:e17236.
- [38] Parthasarathy P, Al-Ansari T, Mackey HR, McKay G. Effect of heating rate on the pyrolysis of camel manure. *Biomass Convers Biorefin* 2023;13:6023–35. <https://doi.org/10.1007/s13399-021-01531-9>.
- [39] Najafi H, Golrokh Sani A, Sobati MA. Thermogravimetric and thermo-kinetic analysis of sugarcane bagasse pith: a comparative evaluation with other sugarcane residues. *Sci Rep* 2024;14:1–22. <https://doi.org/10.1038/s41598-024-52500-x>.
- [40] Zhang Z, Li Y, Luo L, Yellezuome D, Rahman MM, Zou J, et al. Insight into kinetic and Thermodynamic Analysis methods for lignocellulosic biomass pyrolysis. *Renew Energy* 2023;202:154–71. <https://doi.org/10.1016/j.renene.2022.11.072>.
- [41] Clemente-Castro S, Palma A, Ruiz-Montoya M, Giráldez I, Díaz MJ. Optimizing pyrolysis parameters and product analysis of a fluidized bed pilot plant for *Leucaena leucocephala* biomass. *Environ Sci Eur* 2023;35. <https://doi.org/10.1186/s12302-023-00800-w>.
- [42] Nasfi M, Carrier M, Salvador S. Reconsidering the potential of micropyrolyzer to investigate biomass fast pyrolysis without heat transfer limitations. *J Anal Appl Pyrol* 2022;165:105582. <https://doi.org/10.1016/j.jaap.2022.105582>.
- [43] Ascher S, Watson I, You S. Machine learning methods for modelling the gasification and pyrolysis of biomass and waste. *Renew Sustain Energy Rev* 2022;155:111902. <https://doi.org/10.1016/j.rser.2021.111902>.
- [44] Balsora HKSK, Dua V, Joshi JB, Kataria G, Sharma A, et al. Machine learning approach for the prediction of biomass pyrolysis kinetics from preliminary analysis. *J Environ Chem Eng* 2022;10:108025. <https://doi.org/10.1016/j.jece.2022.108025>.
- [45] Aboelela D, Saleh H, Attia AM, Elhenawy Y, Majozi T, Bassyouni M. Recent advances in biomass pyrolysis processes for bioenergy production: optimization of operating conditions. *Sustainability (switzerland)* 2023;15. <https://doi.org/10.3390/su151411238>.
- [46] Huang J, Wang X, Sun Z, Song L, Wang J. Interpretable machine learning model for activation energy prediction based on biomass properties. *Thermal Science and Engineering Progress* 2024;53:102734. <https://doi.org/10.1016/j.tsep.2024.102734>.
- [47] Gupta R, Ouderji ZH, Uzma YZ, Sloan WT, You S. Machine learning for sustainable organic waste treatment: a critical review. *Npj Materials Sustainability* 2024;2:5. <https://doi.org/10.1038/s44296-024-00009-9>.
- [48] Lei J, Ye X, Wang H, Zhao D. Insights into Pyrolysis Kinetics, Thermodynamics, and the Reaction Mechanism of Wheat Straw for Its Resource Utilization. *Sustainability (switzerland)* 2023;15. <https://doi.org/10.3390/su151612536>.
- [49] Osman AI, Nasr M, Farghali M, Rashwan AK, Abdelkader A, Al-Muhtaseb AH, et al. Optimizing Biodiesel Production from Waste with Computational Chemistry, Machine Learning and Policy Insights: a Review 2024;vol. 22. <https://doi.org/10.1007/s10311-024-01700-y>.
- [50] Zhang P, Zhang T, Zhang J, Liu H, Chicaiza-Ortiz C, Lee JTE, et al. A machine learning assisted prediction of potential biochar and its applications in anaerobic digestion for valuable chemicals and energy recovery from organic waste. *Carbon Neutrality* 2024;3. <https://doi.org/10.1007/s43979-023-00078-0>.
- [51] Liu J, Lyu H, Cheng C, Xu Z, Zhang W. Enhancing pyrolysis process monitoring and prediction for biomass: A machine learning approach. *Fuel* 2024;362:130873. <https://doi.org/10.1016/j.fuel.2024.130873>.
- [52] Chinenye Divine D, Hubert S, Epelle EI, Ojo AU, Adeleke AA, Ogbaga CC, et al. Enhancing biomass Pyrolysis: Predictive insights from process simulation integrated with interpretable Machine learning models. *Fuel* 2024;366:131346. <https://doi.org/10.1016/j.fuel.2024.131346>.
- [53] Sánchez-Ávila N, Cardarelli A, Carmona-Cabello M, Dorado MP, Pinzi S, Barbanera M. Kinetic and thermodynamic behavior of co-pyrolysis of olive pomace and thermoplastic waste via thermogravimetric analysis. *Renew Energy* 2024;230. <https://doi.org/10.1016/j.renene.2024.120880>.
- [54] Amoloye MA, Abdulkareem SA, Adeniyi AG. Thermo-kinetics, thermodynamics, and ANN modeling of the pyrolytic behaviours of Corn Cob, Husk, Leaf, and Stalk using thermogravimetric analysis. *Chem Prod Process Model* 2023;18:859–76. <https://doi.org/10.1515/cppm-2023-0021>.
- [55] Chen R, Yu X, Dong B, Dai X. Sludge-to-energy approaches based on pathways that couple pyrolysis with anaerobic digestion (thermal hydrolysis pre/post-treatment): Energy efficiency assessment and pyrolysis kinetics analysis. *Energy* 2020;190. <https://doi.org/10.1016/j.energy.2019.116240>.
- [56] Vanisree GS, Chandran AM, Aparna K. Investigation on thermochemical characteristics and pyrolysis kinetics of lignocellulosic biomass for biofuel production feasibility. *Biomass Convers Biorefin* 2024. <https://doi.org/10.1007/s13399-024-05657-4>.
- [57] Osman AI, Fang B, Zhang Y, Liu Y, Yu J, Farghali M, et al. Life Cycle Assessment and Techno-Economic Analysis of Sustainable Bioenergy Production: a Review 2024;vol. 22. <https://doi.org/10.1007/s10311-023-01694-z>.
- [58] Kumar VK, Hallad SC, Panwar NL. Thermogravimetric pyrolysis investigation of pistachio shell for its potential of thermal properties, kinetics and thermodynamics. *Discover Energy* 2024;4. <https://doi.org/10.1007/s43937-024-00030-y>.
- [59] Rashid JA, Lalung J, Kassim MA, Wijaya D, Allzrag AMM, Shaah MA. Kinetics and thermodynamic studies on biodiesel synthesis via Soxhlet extraction of *Scenedesmus parvus* algae oil. *Energy Conversion and Management: X* 2024;23:100633. <https://doi.org/10.1016/j.ecmx.2024.100633>.
- [60] Lingamdinne LP, Angaru GKR, Pal CA, Koduru JR, Karri RR, Mubarak NM, et al. Insights into kinetics, thermodynamics, and mechanisms of chemically activated sunflower stem biochar for removal of phenol and bisphenol-A from wastewater. *Sci Rep* 2024;14:1–13. <https://doi.org/10.1038/s41598-024-54907-y>.
- [61] Dai M, Guo T, Hu X, Ma J, Guo Q. Simulation of a 1MWth biomass chemical looping gasification process based on kinetic and pyrolysis models. *Int J Hydrogen Energy* 2024;80:298–307. <https://doi.org/10.1016/j.ijhydene.2024.07.154>.
- [62] Temireyeva A, Sarbassov Y, Shah D. Process simulation of flax straw pyrolysis with kinetic reaction Model: Experimental validation and exergy analysis. *Fuel* 2024;367:131494. <https://doi.org/10.1016/j.fuel.2024.131494>.
- [63] Nath S. Biotechnology and biofuels: paving the way towards a sustainable and equitable energy for the future. *Discover Energy* 2024;4. <https://doi.org/10.1007/s43937-024-00032-w>.
- [64] Samuel Oluhengba O, Goodness Adeleye P, Blessing Oladipupo S, Timothy Adeleye A, Igenepo JK. Biomass-derived biochar in wastewater treatment- a circular economy approach. *Waste Management Bulletin* 2024;1:1–14. <https://doi.org/10.1016/j.wmb.2023.07.007>.

- [65] Wachter I, Rantuch P, Drienovský M, Martinka J, Ház A, Štefko T. Determining the Activation Energy of Spent Coffee Grounds By the Thermogravimetric Analysis. *Journal of Chemical Technology and Metallurgy* 2022;57:1006–18.
- [66] Nam NH, Ngoc CTA, Van Bay T. Investigation on gasification of coffee husk in CO₂, H₂O, and mixed atmospheres. *Vietnam Journal of Chemistry* 2021;59:775–80. <https://doi.org/10.1002/vjch.202100002>.
- [67] Chaiklangmuang S, Kurosawa K, Li L, Morishita K, Takarada T. Thermal degradation behavior of coffee residue in comparison with biomasses and its product yields from gasification. *J Energy Inst* 2015;88:323–31. <https://doi.org/10.1016/j.joei.2014.08.001>.
- [68] Xavier TP, Lira TS, Schettino MA, Barrozo MAS. A study of pyrolysis of Macadamia Nut Shell: Parametric sensitivity analysis of the IPR model. *Braz J Chem Eng* 2016;33:115–22. <https://doi.org/10.1590/0104-6632.20160331s00003629>.
- [69] Linh VN, Van Dong N, Nam NH. Investigation on gasification of agricultural wastes: the case of macadamia husk. *Vietnam Journal of Chemistry* 2021;59:599–605. <https://doi.org/10.1002/vjch.202100011>.
- [70] Bhattarai A, Kemp A, Jahromi H, Kafle S, Adhikari S. Thermochemical Characterization and Kinetics of Biomass, Municipal Plastic Waste, and Coal Blends and Their Potential for Energy Generation via Gasification. *ACS Omega* 2023;8:45985–6001. <https://doi.org/10.1021/acsomega.3c06849>.
- [71] Ko KH, Rawal A, Sahajwalla V. Analysis of thermal degradation kinetics and carbon structure changes of co-pyrolysis between macadamia nut shell and PET using thermogravimetric analysis and ¹³C solid state nuclear magnetic resonance. *Energ Conver Manage* 2014;86:154–64. <https://doi.org/10.1016/j.enconman.2014.04.060>.
- [72] Kumar M, Mishra PK, Upadhyay SN. Thermal degradation of rice husk: Effect of pre-treatment on kinetic and thermodynamic parameters. *Fuel* 2020;268. <https://doi.org/10.1016/j.fuel.2020.117164>.
- [73] Kamruzzaman M, Shahriyar M, Bhuiyan AA, Bhattacharjya DK, Islam MK, Alam E. Energy potential of biomass from rice husks in bangladesh: An experimental study for thermochemical and physical characterization. *Energy Rep* 2024;11:3450–60. <https://doi.org/10.1016/j.egy.2024.03.019>.
- [74] Alaba PA, Popoola SI, Abnisa F, Lee CS, Ohunakin OS, Adetiba E, et al. Thermal decomposition of rice husk: a comprehensive artificial intelligence predictive model. *J Therm Anal Calorim* 2020;140:1811–23. <https://doi.org/10.1007/s10973-019-08915-0>.
- [75] Alashmawy MM, Hassan HS, Ookawara SA, Elwardany AE. Thermal decomposition characteristics and study of the reaction kinetics of tea-waste. *Biomass Convers Biorefin* 2023;13:9487–505. <https://doi.org/10.1007/s13399-023-04017-y>.
- [76] Çakmak TG, Saricaoglu B, Ozkan G, Tomas M, Capanoglu E. Valorization of tea waste: Composition, bioactivity, extraction methods, and utilization. *Food Sci Nutr* 2024;12:3112–24. <https://doi.org/10.1002/fsn3.4011>.
- [77] Mamadou Seydou B, Himbani PB, Ndiaye LG. Determination and comparison of combustion kinetics parameters of peanut shells, cashew nut shells, palm nut shells, and millet stem. 2022 IEEE Multi-conference on Natural and Engineering Sciences for Sahel's Sustainable Development (MNE3SD), IEEE; 2022, p. 1–7. Doi: 10.1109/MNE3SD53781.2022.9723216.
- [78] Kumar M, Rai D, Bhardwaj G, Upadhyay SN, Mishra PK. Pyrolysis of peanut shell: Kinetic analysis and optimization of thermal degradation process. *Ind Crop Prod* 2021;174:114128. <https://doi.org/10.1016/j.indcrop.2021.114128>.
- [79] Lei J, Liu X, Xu B, Liu Z, Fu Y. Combustion characteristics, kinetics and thermodynamics of peanut shell for its bioenergy valorization. *Processes* 2024;12:1022. <https://doi.org/10.3390/pr12051022>.
- [80] Parthasarathy P, Tahir F, Pradhan S, Al-Ansari T, McKay G. Life cycle assessment of biofuel production from waste date stones using conventional and microwave pyrolysis. *Energy Conversion and Management: X* 2024;21:100510. <https://doi.org/10.1016/j.ecmx.2023.100510>.
- [81] Ochieng R, Cerón AL, Konist A, Sarker S. A combined analysis of the drying and decomposition kinetics of wood pyrolysis using non-isothermal thermogravimetric methods. *Energy Conversion and Management: X* 2023;20. <https://doi.org/10.1016/j.ecmx.2023.100424>.
- [82] Lubwama M, Yiga VA. Development of groundnut shells and bagasse briquettes as sustainable fuel sources for domestic cooking applications in Uganda. *Renew Energy* 2017. <https://doi.org/10.1016/j.renene.2017.04.041>.
- [83] Shen J, Zhu S, Liu X, Zhang H, Tan J. The prediction of elemental composition of biomass based on proximate analysis. *Energ Conver Manage* 2010;51:983–7. <https://doi.org/10.1016/j.enconman.2009.11.039>.
- [84] Parikh J, Channiwala SA, Ghosal GK. A correlation for calculating elemental composition from proximate analysis of biomass materials. *Fuel* 2007;86:1710–9. <https://doi.org/10.1016/j.fuel.2006.12.029>.
- [85] Ghugare SB, Tiwary S, Tambe SS. Computational intelligence based models for prediction of elemental composition of solid biomass fuels from proximate analysis. *International Journal of System Assurance Engineering and Management* 2017;8:2083–96. <https://doi.org/10.1007/s13198-014-0324-4>.
- [86] Hosokai S, Matsuoka K, Kuramoto K, Suzuki Y. Modification of Dulong's formula to estimate heating value of gas, liquid and solid fuels. *Fuel Process Technol* 2016;152:399–405. <https://doi.org/10.1016/j.fuproc.2016.06.040>.
- [87] Channiwala SA, Parikh PP. A unified correlation for estimating HHV of solid, liquid and gaseous fuels. *Fuel* 2002;81:1051–63. [https://doi.org/10.1016/S0016-2361\(01\)00131-4](https://doi.org/10.1016/S0016-2361(01)00131-4).
- [88] Huang YF, Lo SL. Predicting heating value of lignocellulosic biomass based on elemental analysis. *Energy* 2020;191:116501. <https://doi.org/10.1016/j.energy.2019.116501>.
- [89] El-Sayed SA, Khass TM, Mostafa ME. Thermal degradation behaviour and chemical kinetic characteristics of biomass pyrolysis using TG/DTG/DTA techniques. *Biomass Convers Biorefin* 2024;14:20–40. <https://doi.org/10.1007/s13399-023-03926-2>.
- [90] Han Y, Li H. A new, improved method to identify reaction mechanisms based on the shape of derivative thermogravimetric curves. *Case Studies in Thermal Engineering* 2023;45:102993. <https://doi.org/10.1016/j.csite.2023.102993>.
- [91] Zhang J, Liu J, Evrendilek F, Zhang X, Buyukada M. TG-FTIR and Py-GC/MS analyses of pyrolysis behaviors and products of cattle manure in CO₂ and N₂ atmospheres: Kinetic, thermodynamic, and machine-learning models. *Energ Conver Manage* 2019;195:346–59. <https://doi.org/10.1016/j.enconman.2019.05.019>.
- [92] Ben Abdallah A, Ben Hassen Trabelsi A, Navarro MV, Veses A, García T, Mihoubi D. Pyrolysis of tea and coffee wastes: effect of physicochemical properties on kinetic and thermodynamic characteristics. *J Therm Anal Calorim* 2023;148:2501–15. <https://doi.org/10.1007/s10973-022-11878-4>.
- [93] Parthasarathy P, Fernandez A, Al-Ansari T, Mackey HR, Rodriguez R, McKay G. Thermal degradation characteristics and gasification kinetics of camel manure using thermogravimetric analysis. *J Environ Manage* 2021;287:112345. <https://doi.org/10.1016/j.jenvman.2021.112345>.
- [94] Shahdan NA, Balasundram V, Ibrahim N, Isha R, Manan ZA. Catalytic Co-pyrolysis of empty fruit bunch and high-density polyethylene mixtures over rice husk ash: Thermogravimetric, kinetic and thermodynamic analyses. *Cleaner Engineering and Technology* 2022;9:100538. <https://doi.org/10.1016/j.clet.2022.100538>.
- [95] Nie Y, Song X, Shan M, Yang X. Effect of pelletization on biomass thermal degradation in combustion: A case study of peanut shell and wood sawdust using macro-TGA. *Energy and Built Environment* 2024. <https://doi.org/10.1016/j.enbenv.2024.04.002>.
- [96] El-Sayed SA, Mostafa ME. Thermal pyrolysis and kinetic parameter determination of mango leaves using common and new proposed parallel kinetic models. *RSC Adv* 2020;10:18160–79. <https://doi.org/10.1039/d0ra00493f>.
- [97] Yi Q, Qi F, Cheng G, Zhang Y, Xiao B, Hu Z, et al. Thermogravimetric analysis of co-combustion of biomass and biochar. *J Therm Anal Calorim* 2013;112:1475–9. <https://doi.org/10.1007/s10973-012-2744-1>.
- [98] Huang H, Liu J, Liu H, Evrendilek F, Buyukada M. Pyrolysis of water hyacinth biomass parts: Bioenergy, gas emissions, and by-products using TG-FTIR and Py-GC/MS analyses. *Energ Conver Manage* 2020;207:112552. <https://doi.org/10.1016/j.enconman.2020.112552>.
- [99] Zhang J, Jin J, Wang M, Naidu R, Liu Y, Man YB, et al. Co-pyrolysis of sewage sludge and rice husk/ bamboo sawdust for biochar with high aromaticity and low metal mobility. *Environ Res* 2020;191:110034. <https://doi.org/10.1016/j.envres.2020.110034>.
- [100] Gajera B, Tyagi U, Sarma AK, Jha MK. Impact of torrefaction on thermal behavior of wheat straw and groundnut stalk biomass: Kinetic and thermodynamic study. *Fuel Communications* 2022;12:100073. <https://doi.org/10.1016/j.fucom.2022.100073>.
- [101] Gupta GK, Gupta PK, Mondal MK. Experimental process parameters optimization and in-depth product characterizations for teak sawdust pyrolysis. *Waste Manag* 2019;87:499–511. <https://doi.org/10.1016/j.wasman.2019.02.035>.
- [102] Yousef S, Eimontas J, Striugas N, Subadra SP, Abdelnaby MA. Thermal degradation and pyrolysis kinetic behaviour of glass fibre-reinforced thermoplastic resin by TG-FTIR, Py-GC/MS, linear and nonlinear isoconversional models. *J Mater Res Technol* 2021;15:5360–74. <https://doi.org/10.1016/j.jmrt.2021.11.011>.
- [103] Ahmed SF, Rafa SJ, Mehjabin A, Tasannum N, Ahmed S, Mofijur M, et al. Bio-oil from microalgae: Materials, production, technique, and future. *Energy Rep* 2023;10:3297–314. <https://doi.org/10.1016/j.egy.2023.09.068>.
- [104] Igliński B, Kujawski W, Kielkowska U. Pyrolysis of Waste Biomass: Technical and Process Achievements. And Future Development—A Review *Energies* 2023;16. <https://doi.org/10.3390/en16041829>.
- [105] Vyazovkin S, Muravyev N. Single heating rate methods are a faulty approach to pyrolysis kinetics. *Biomass Convers Biorefin* 2024;14:16879–81. <https://doi.org/10.1007/s13399-022-03735-z>.
- [106] Uddin Monir M, Muntasir Shovon S, Ahamed Akash F, Habib MA, Techato K, Abd Aziz A, et al. Comprehensive characterization and kinetic analysis of coconut shell thermal degradation: Energy potential evaluated via the Coats-Redfern method. *Case Studies in Thermal Engineering* 2024;55:104186. <https://doi.org/10.1016/j.csite.2024.104186>.
- [107] Mishra RK, Vinu R. Pyrolysis characteristics and kinetic investigation of waste groundnut shells using thermogravimetric analyzer, Py-FTIR, and Py-GC-MS. *J Anal Appl Pyrol* 2024;179:106514. <https://doi.org/10.1016/j.jaap.2024.106514>.
- [108] Gajera ZR, Verma K, Tekade SP, Sawarkar AN. Kinetics of co-gasification of rice husk biomass and high sulphur petroleum coke with oxygen as gasifying medium via TGA. *Bioresource Technology Reports* 2020;11:100479. <https://doi.org/10.1016/j.biteb.2020.100479>.
- [109] Balasundram V, Ibrahim N, Kasmani RM, Hamid MKA, Isha R, Hasbullah H, et al. Thermogravimetric catalytic pyrolysis and kinetic studies of coconut copra and rice husk for possible maximum production of pyrolysis oil. *J Clean Prod* 2017;167:218–28. <https://doi.org/10.1016/j.jclepro.2017.08.173>.
- [110] Raza M, Abu-Jdayil B. Synergic interactions, kinetic and thermodynamic analyses of date palm seeds and cashew shell waste co-pyrolysis using Coats-Redfern method. *Case Studies in Thermal Engineering* 2023;47:103118. <https://doi.org/10.1016/j.csite.2023.103118>.

- [111] Yu J, Zeng X, Zhang J, Zhong M, Zhang G, Wang Y, et al. Isothermal differential characteristics of gas-solid reaction in micro-fluidized bed reactor. *Fuel* 2013;103: 29–36. <https://doi.org/10.1016/j.fuel.2011.09.060>.
- [112] Khawam A, Flanagan DR. Solid-state kinetic models: Basics and mathematical fundamentals. *J Phys Chem B* 2006;110:17315–28. <https://doi.org/10.1021/jp062746a>.
- [113] Almusafir R, Smith JD. Thermal Decomposition and Kinetic Parameters of Three Biomass Feedstocks for the Performance of the Gasification Process Using a Thermogravimetric Analyzer. *Energies* 2024;17. <https://doi.org/10.3390/en17020396>.
- [114] Silva J, Teixeira S, Teixeira J. A Review of Biomass Thermal Analysis, Kinetics and Product Distribution for Combustion Modeling : From the Micro to Macro Perspective. *Energies* 2023;16. <https://doi.org/10.3390/en16186705>.
- [115] Sribala G, Vargas DC, Kostetskyy P, Van De VR, Broadbelt LJ, Marin GB, et al. New Perspectives into Cellulose Fast Pyrolysis Kinetics Using a Py- GC × GC-FID / MS System. *ACS Engineering* 2022;2:320–32. <https://doi.org/10.1021/acseengineeringau.2c00006>.
- [116] Sbirrazzuoli N. Determination of pre-exponential factor and reaction mechanism in a model-free way. *Thermochim Acta* 2020;178707. <https://doi.org/10.1016/j.tca.2020.178707>.
- [117] Hai A, Bharath G, Daud M, Rambabu K, Ali I, Hasan SW, et al. Valorization of groundnut shell via pyrolysis: Product distribution, thermodynamic analysis, kinetic estimation, and artificial neural network modeling. *Chemosphere* 2021; 283:131162. <https://doi.org/10.1016/j.chemosphere.2021.131162>.
- [118] Balogun AO, Adeleke AA, Ikubanni PP, Adegoke SO, Alayat AM, McDonald AG. Kinetics modeling, thermodynamics and thermal performance assessments of pyrolytic decomposition of Moringa oleifera husk and Delonix regia pod. *Sci Rep* 2021;11:1–12. <https://doi.org/10.1038/s41598-021-93407-1>.
- [119] Ali I, Tariq R, Naqvi SR, Khoja AH, Mehran MT, Naqvi M, et al. Kinetic and thermodynamic analyses of dried oily sludge pyrolysis. *J Energy Inst* 2021;95: 30–40. <https://doi.org/10.1016/j.joiei.2020.12.002>.
- [120] Vyazovkin S, Burnham AK, Criado JM, Pérez-Maqueda LA, Popescu C, Sbirrazzuoli N. ICTAC Kinetics Committee recommendations for performing kinetic computations on thermal analysis data. *Thermochim Acta* 2011;520:1–19. <https://doi.org/10.1016/j.tca.2011.03.034>.
- [121] Álvarez A, Pizarro C, García R, Bueno JL, Lavín AG. Determination of kinetic parameters for biomass combustion. *Bioresour Technol* 2016;216:36–43. <https://doi.org/10.1016/j.biortech.2016.05.039>.
- [122] Adeoye AO, Quadri RO, Lawal OS. Wet synthesis, characterization of goethite nanoparticles and its application in catalytic pyrolysis of palm kernel shell in TGA. *Results in Surfaces and Interfaces* 2023;11:100118. <https://doi.org/10.1016/j.rsufi.2023.100118>.
- [123] Petrović A, Stergar J, Škodić L, Rašl N, Cenčić Predikaka T, Čuček L, et al. Thermo-kinetic analysis of pyrolysis of thermally pre-treated sewage sludge from the food industry. *Thermal Science and Engineering Progress* 2023;42. Doi: 10.1016/j.tsep.2023.101863.
- [124] Cai H, Liu J, Xie W, Kuo J, Buyukada M, Evrendilek F. Pyrolytic kinetics, reaction mechanisms and products of waste tea via TG-FTIR and Py-GC/MS. *Energ Conver Manage* 2019;184:436–47. <https://doi.org/10.1016/j.enconman.2019.01.031>.
- [125] Márquez A, Patlaka E, Sfakiotakis S, Ortiz I, Sánchez-Hervás JM. Pyrolysis of municipal solid waste: A kinetic study through multi-step reaction models. *Waste Manag* 2023;172:171–81. <https://doi.org/10.1016/j.wasman.2023.10.031>.
- [126] Collins S, Ghodke P. Kinetic parameter evaluation of groundnut shell pyrolysis through use of thermogravimetric analysis. *J Environ Chem Eng* 2018;6:4736–42. <https://doi.org/10.1016/j.jece.2018.07.012>.
- [127] Xu Z, Xiao X, Fang P, Ye L, Huang J, Wu H, et al. Comparison of combustion and pyrolysis behavior of the peanut shells in air and N₂: Kinetics, thermodynamics and gas emissions. *Sustainability (Switzerland)* 2020;12. Doi: 10.3390/su12020464.
- [128] Yiga VA, Katamba M, Lubwama M, Adolffson KH, Hakkarainen M, Kamalha E. Combustion, kinetics and thermodynamic characteristics of rice husks and rice husk-biocomposites using thermogravimetric analysis. *J Therm Anal Calorim* 2023;148:11435–54. <https://doi.org/10.1007/s10973-023-12458-w>.
- [129] Choudhary J, Alawa B, Chakma S. Insight into the kinetics and thermodynamic analyses of co-pyrolysis using advanced isoconversional method and thermogravimetric analysis: A multi-model study of optimization for enhanced fuel properties. *Process Saf Environ Prot* 2023;173:507–28. <https://doi.org/10.1016/j.psep.2023.03.033>.
- [130] Ma C, Zhang F, Hu J, Wang H, Yang S, Liu H. Co-pyrolysis of sewage sludge and waste tobacco stem: Gas products analysis, pyrolysis kinetics, artificial neural network modeling, and synergistic effects. *Bioresour Technol* 2023;389:129816. <https://doi.org/10.1016/j.biortech.2023.129816>.